

# Analysis-aware defeaturing: first results

A. Buffa<sup>1,2</sup>, O. Chanon<sup>1</sup>, R. Vázquez Hernández<sup>1,2</sup>

<sup>1</sup> MNS, Institute of Mathematics, École Polytechnique Fédérale de Lausanne, Switzerland

<sup>2</sup> Istituto di Matematica Applicata e Tecnologie Informatiche ‘E. Magenes’ (CNR), Pavia, Italy

May 25, 2022

---

## Abstract

Defeating consists in simplifying geometrical models by removing the geometrical features that are considered not relevant for a given simulation. Feature removal and simplification of computer-aided design models enables faster simulations for engineering analysis problems, and simplifies the meshing problem that is otherwise often unfeasible. The effects of defeating on the analysis are then neglected and, as of today, there are basically very few, if not none, strategies to quantitatively evaluate such an impact. Understanding well the effects of this process is an important step for automatic integration of design and analysis. We formalize the process of defeating by understanding its effect on the solution of the Laplace equation defined on the geometrical model of interest, with Neumann boundary conditions on the features themselves. We derive an a posteriori estimator of the energy error between the solutions of the exact and the defeated geometries in  $\mathbb{R}^n$ , that is simple, efficient and reliable up to oscillations. The dependence of the estimator upon the size of the features is explicit, and the effectivity index is independent from the number of features considered.

## 1 Introduction

Complex geometrical models are created and processed using computer-aided design tools (CAD) in the context of computer-aided engineering. The automatic integration of design and analysis tools in a single workflow has been an important topic of research for many years. One of the methodologies that emerged in the last 15 years is the one based on isogeometric analysis (IGA) [1, 2], a method to solve partial differential equations (PDEs) using smooth B-splines, NURBS or variances thereof as basis functions for the solution field. IGA has proved to be a valid simulation method in a wide range of applications [3], and a sound mathematical theory [4, 5], including strategies for adaptive refinement [6–9], is now available.

However, a major challenge remains in the usability of complex CAD geometries in the analysis phase. While the first CAD models used in IGA were relatively simple geometries defined by multiple patches [2, 10], in recent years, more effort is being dedicated to the analysis on complex geometries defined via Boolean operations such as trimming [11–13] and union [14–16]. The related engineering literature includes in particular the shell analysis on models with B-reps [17, 18], and the finite cell method combined with IGA on complex geometries [19–21]. Before even doing any simulation on complex geometries, defining them may already require a very large number of degrees of freedom, that are not necessarily needed - and potentially too costly to take into account - to perform an accurate analysis. Moreover, repeated design changes is part of a typical process in simulation-based design for manufacturing, and it involves adding or removing geometrical features to the design, as well as adjusting geometric parameters in order to meet functionality, manufacturability and aesthetic requirements. Therefore, to be able to consider complex geometries and to accelerate the process of analysis-aware geometric design, it is essential to be able to simplify the geometrical model, process also called defeating, while understanding its effect on the solution of the problem in hand. The idea of defeating is illustrated in Figure 1, where we show a complex geometry and its simplified version, with all the features removed.

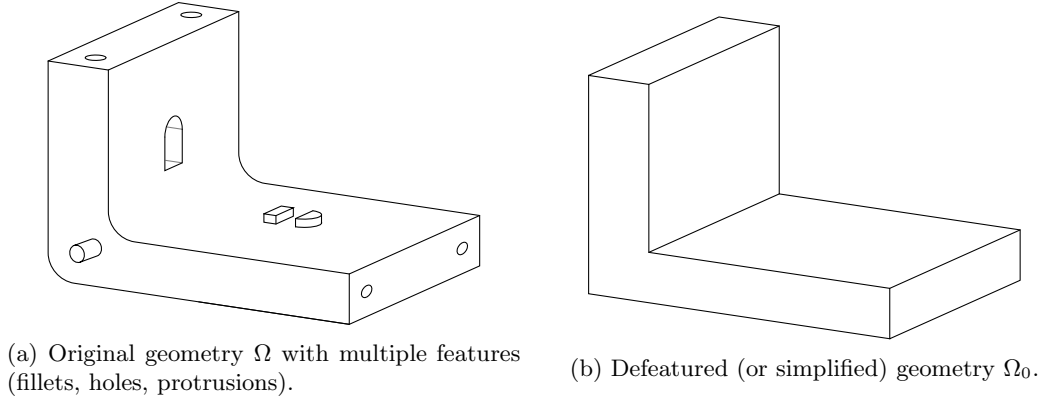


Figure 1: Illustration of defeaturing.

For a long time, the defeaturing problem has been approached using some subjective a priori criteria, relying mostly on the engineers' expertise or based on geometrical considerations such as variations in volume or area of the domain [22]. More objective criteria have then been considered, still based on some a priori knowledge of the mechanical problem at hand such as the verification of constitutive or conservation laws [23, 24]. However, in order to automatize the simulation-based design process, the interest is to have an a posteriori criterion to assess the error introduced by defeaturing from the result of the analysis in the defeated geometric model. Following this direction, an a posteriori criterion is given in [25]: it evaluates an approximation of the energy norm between the exact solution of the problem at hand and the solution on the defeated geometry. It is intuitively based on the fact that the energy error due to defeaturing is concentrated in the modified boundaries of the geometry, and this boundary error is estimated by solving local problems around each feature. Nevertheless, this approach does not give a demonstrated certification that the proposed criterion is indeed a good estimator of the defeaturing error.

A different approach is based on the concept of feature sensitivity analysis (FSA) [26, 27], which relies on topological sensitivity analysis [28, 29], a method used in design optimization that studies the impact of infinitesimal (topological) geometrical changes on the solution of a given PDE. The works on FSA study the defeaturing in geometries with a single feature which is arbitrarily-shaped. First order changes of quantities of interest are analyzed when a small, internal or boundary, hole is removed from the geometry. However, the main drawbacks of FSA come from the assumption that features must be of infinitesimal size, and that it is not adapted for geometries for which a protrusion is removed from the model (see again Figure 1).

An alternative approach, still based on a posteriori error estimators, is proposed in [30] for internal holes. The idea behind this estimator is to reformulate the geometrical defeaturing error as a modeling error, by rewriting the PDE solved in two different geometries as two different PDEs on a unique geometry. The modeling error is then estimated using the dual weighted residual method introduced in [31, 32], following the lines of [33, 34] that study heterogeneous and perforated materials, and [35] that studies the error introduced by the approximation of boundary conditions, two problems that can be easily related to defeaturing. This a posteriori approach has then been generalized to different linear and non-linear problems, and to other types of features, in [36–39]. However, some heuristic remains in all these contributions, and a precise mathematical study of the estimator with regards to its efficiency and stability is lacking. In particular, it is assumed that the difference between the solutions of the PDE in the exact and defeated geometries is small, and it relies on the heuristic estimation of constants that depend on the size of the features, but are not explicit with respect to it.

Consequently, the first aim of this paper is to give a solid mathematical framework for analysis-based defeaturing, and to precisely define the defeaturing error, in energy norm, in the context of the Laplace equation for which Neumann boundary conditions are imposed on the features. We introduce an a posteriori estimator of the defeaturing error that explicitly depends on the features' size and that is independent from

the number of features present in the geometry. A similar estimator is derived in [40], but for the case in which the computational domain is approximated by a discretization (a triangulation) which does not resolve all the geometrical features, and the geometry only contains negative features. In our case, the considered features are very general, they can either be negative (internal or boundary holes) or positive (protrusions), and they can share part of their boundary with the exact domain. Moreover, the defeaturing is not necessarily due to some geometry discretization.

Our second goal is to prove that the proposed estimator is both an upper and a lower bound for the defeaturing error, that is, we analyze its reliability and its efficiency to be able to use it in a single workflow that links geometric modeling and isogeometric simulation, allowing us to decide whether to add or get rid of any feature after the result of a simulation. The a posteriori estimator is simple, efficient, reliable up to oscillations, computationally cheap and naturally parallelizable; it only requires the computation of the solution in the defeatured domain, the solution of a local problem in (an extension of) each positive feature, and the evaluation of the error made on the normal derivative of the solution on specific boundaries, that is, the computation of local boundary integrals.

After introducing in Section 2 the notation used throughout the article, we precisely define the defeaturing problem in Section 3. Then, in Section 4, the defeaturing error estimator is derived and analyzed, first in the case in which the geometry contains a single negative feature, then in the case of a single positive feature, and finally in the multi-feature case required by complex geometric models. Subsequently, in Section 5, we present a validation of the results presented previously. Our validation is obtained by comparing errors and defeaturing estimators for numerical solutions on very fine meshes. We finally draw conclusions in Section 6

## 2 Notation

We start by introducing the notation that will be used throughout the paper. Let  $n = 2$  or  $n = 3$ , let  $\omega$  be any open  $k$ -dimensional manifold in  $\mathbb{R}^n$ ,  $k \leq n$ , and let  $\varphi \subset \partial\omega$ .

We denote by  $|\omega|$ ,  $\bar{\omega}$ ,  $\text{int}(\omega)$ ,  $\text{diam}(\varphi)$  and  $\text{hull}(\varphi)$ , respectively, the measure of  $\omega$ , its closure, its interior, the diameter of  $\varphi$  along the manifold  $\partial\omega$ , and the convex hull of  $\varphi$  in the manifold  $\partial\omega$ . Moreover, let  $H^s(\omega)$  denote the Sobolev space of order  $s \in \mathbb{R}$  whose classical norm and semi-norm are written  $\|\cdot\|_{s,\omega}$  and  $|\cdot|_{s,\omega}$ , respectively. We recall from [41, Definition 1.3.2.1], that for all  $z \in H^s(\omega)$  with  $\theta := s - \lfloor s \rfloor$ ,

$$\|z\|_{s,\omega}^2 := \|z\|_{\lfloor s \rfloor,\omega}^2 + |z|_{\theta,\omega}^2; \quad |z|_{\theta,\omega}^2 := \int_{\omega} \int_{\omega} \frac{(z(x) - z(y))^2}{|x - y|^{k+2\theta}} dx dy.$$

We also write  $L^2(\omega) := H^0(\omega)$ , and for some  $z \in H^{\frac{1}{2}}(\varphi)$ ,  $H_{z,\varphi}^1(\omega) := \{y \in H^1(\omega) : \text{tr}_{\varphi}(y) = z\}$ , where  $\text{tr}_{\varphi}(y)$  denotes the trace of  $y$  on  $\varphi \subset \partial\omega$ . Moreover, we consider the Sobolev space

$$H_{00}^{\frac{1}{2}}(\varphi) = \left\{ z \in L^2(\varphi) : z^* \in H^{\frac{1}{2}}(\partial\omega) \right\},$$

where  $z^*$  is the extension of  $z$  by 0 on  $\partial\omega$ , with its norm and semi-norm that we respectively denote  $\|\cdot\|_{H_{00}^{\frac{1}{2}}(\varphi)}$  and  $|\cdot|_{H_{00}^{\frac{1}{2}}(\varphi)}$ . We recall from [41, Lemma 1.3.2.6], that there are two constants  $C \geq c > 0$  such that for all  $z \in H_{00}^{\frac{1}{2}}(\varphi)$ ,

$$\|z\|_{H_{00}^{1/2}(\varphi)}^2 := \|z\|_{\frac{1}{2},\varphi}^2 + |z|_{H_{00}^{1/2}(\varphi)}^2, \quad \text{where} \quad c|z|_{H_{00}^{1/2}(\varphi)}^2 \leq \int_{\varphi} \frac{z^2(s)}{\text{dist}(s, \partial\varphi)} ds \leq C|z|_{H_{00}^{1/2}(\varphi)}^2,$$

and from [41, equation (1,3,2,7)],  $\|z\|_{H_{00}^{1/2}(\varphi)} = \|z^*\|_{\frac{1}{2},\partial\omega}$ . In particular,  $|z|_{\frac{1}{2},\omega}^2 + |z|_{H_{00}^{1/2}(\varphi)}^2 = |z^*|_{\frac{1}{2},\partial\omega}^2$ . Furthermore, let  $H_{00}^{-\frac{1}{2}}(\varphi)$  be the dual space of  $H_{00}^{\frac{1}{2}}(\varphi)$  equipped with the dual norm written  $\|\cdot\|_{H_{00}^{-1/2}(\varphi)}$ . Finally, for  $\mathbf{m} = (m_1, \dots, m_n) \in \mathbb{N}^n$ , let  $\mathbb{Q}_{\mathbf{m}}(\omega)$  be the set of polynomials on  $\omega$  of degree  $m_i$  in space direction  $i$ , for  $i = 1, \dots, n$ , and if  $\{\omega_{\ell}\}_{\ell=1}^L$  is a given partition of  $\omega$  such that each  $\omega_{\ell}$  is a straight line if  $k = 1$  or a straight square or triangle if  $k = 2$ , let  $\mathbb{Q}_{\mathbf{m},0}^{\text{pw}}(\omega)$  be the set of continuous functions  $q$  such that  $q|_{\partial\omega} \equiv 0$ ,  $q|_{\omega_{\ell}} \in \mathbb{Q}_{\mathbf{m}}(\omega_{\ell})$  for all  $\ell = 1, \dots, L$ .

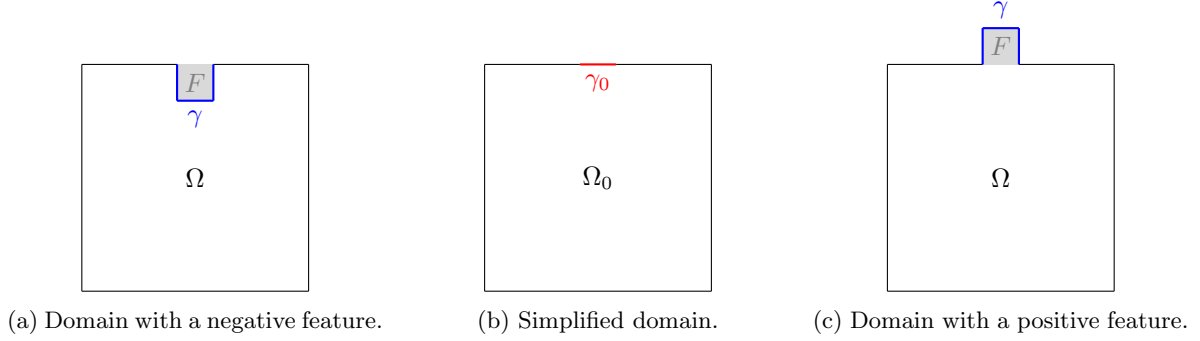


Figure 2: Example of geometries with a negative or a positive feature. In this example, the same simplified geometry  $\Omega_0$  is chosen in both cases.

### 3 Defeaturing problem

In this section, the considered defeaturing problem is stated, together with the notation that will be used throughout the article.

Let us consider a given open Lipschitz domain  $\Omega \subset \mathbb{R}^n$  that can potentially be complex: it may contain geometrical features, that is geometrical details of smaller scale. There exist two kinds of such geometrical features: a feature  $F \subset \mathbb{R}^n$  is said to be

- negative if  $(\overline{F} \cap \overline{\Omega}) \subset \partial\Omega$ ;
- positive if  $F \subset \Omega$ .

A positive feature corresponds to the addition of some material, while a negative feature corresponds to a part where some material has been removed, as illustrated in Figure 2. For now, let us consider a domain  $\Omega$  with one single feature  $F$ , that we suppose to be an open Lipschitz domain. Let  $\Omega_0 \subset \mathbb{R}^n$  be the defeated (or simplified) geometry, that is

- if  $F$  is negative,  $\Omega_0 := \text{int}(\overline{\Omega} \cup \overline{F})$ ;
- if  $F$  is positive,  $\Omega_0 := \Omega \setminus \overline{F}$ ,

and we also assume that  $\Omega_0$  is an open Lipschitz domain.

Let  $\mathbf{n}$ ,  $\mathbf{n}_0$  and  $\mathbf{n}_F$  be the unitary outward normals of  $\Omega$ ,  $\Omega_0$  and  $F$  respectively. Let  $\partial\Omega = \overline{\Gamma_D} \cup \overline{\Gamma_N}$ ,  $\Gamma_D \cap \Gamma_N = \emptyset$ , and we assume that  $\Gamma_D \cap \partial F = \emptyset$ . Finally, let  $\gamma_0 := \partial F \setminus \overline{\Gamma_N} \subset \partial\Omega_0$  and  $\gamma := \partial F \setminus \overline{\gamma_0} \subset \partial\Omega$  so that  $\partial F = \overline{\gamma} \cup \overline{\gamma_0}$  and  $\gamma \cap \gamma_0 = \emptyset$ . See Figure 2.

Note that an internal feature  $F$  is a negative feature, where  $\gamma = \partial F$  and  $\gamma_0 = \emptyset$ . In the following, the defeaturing problem is stated, and the cases in which  $F$  is either positive or negative are treated separately.

Let  $h \in H^{\frac{3}{2}}(\Gamma_D)$ ,  $g \in H^{\frac{1}{2}}(\Gamma_N)$  and  $f \in L^2(\Omega)$ . The problem considered is Poisson equation on the exact geometry  $\Omega$ : find  $u \in H^1(\Omega)$ , the weak solution of

$$\begin{cases} -\Delta u = f & \text{in } \Omega \\ u = h & \text{on } \Gamma_D \\ \frac{\partial u}{\partial \mathbf{n}} = g & \text{on } \Gamma_N, \end{cases} \quad (1)$$

that is,  $u \in H_{h,\Gamma_D}^1(\Omega)$  satisfies for all  $v \in H_{0,\Gamma_D}^1(\Omega)$ ,

$$\int_{\Omega} \nabla u \cdot \nabla v \, dx = \int_{\Omega} f v \, dx + \int_{\Gamma_N} g v \, ds. \quad (2)$$

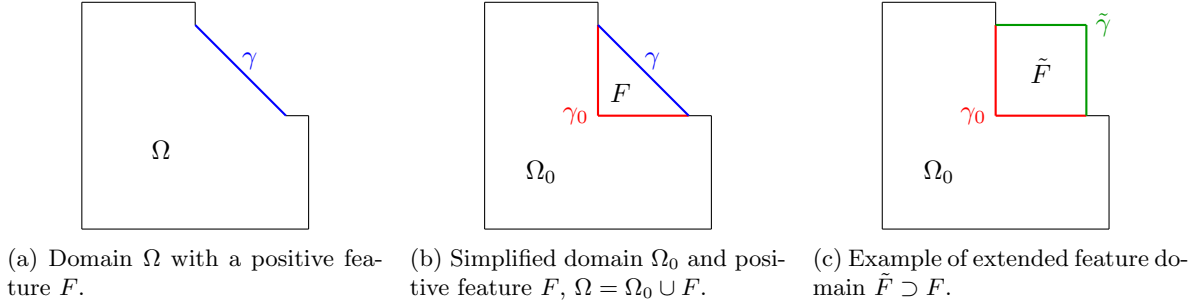


Figure 3: Example of geometry with a positive feature.

Consider any  $L^2$ -extension of  $f$  in  $F$ , that we still write  $f \in L^2(\Omega \cup F)$  by abuse of notation. Instead of (1), the following defeatured (or simplified) problem is solved: given  $g_0 \in H^{\frac{1}{2}}(\gamma_0)$ , find the weak solution  $u_0 \in H^1(\Omega_0)$  of

$$\begin{cases} -\Delta u_0 = f & \text{in } \Omega_0 \\ u_0 = h & \text{on } \Gamma_D \\ \frac{\partial u_0}{\partial \mathbf{n}_0} = g & \text{on } \Gamma_N \setminus \gamma \\ \frac{\partial u_0}{\partial \mathbf{n}_0} = g_0 & \text{on } \gamma_0, \end{cases} \quad (3)$$

that is  $u_0 \in H_{h,\Gamma_D}^1(\Omega_0)$  satisfies for all  $v \in H_{0,\Gamma_D}^1(\Omega_0)$ ,

$$\int_{\Omega_0} \nabla u_0 \cdot \nabla v \, dx = \int_{\Omega_0} f v \, dx + \int_{\Gamma_N \setminus \gamma} g v \, ds + \int_{\gamma_0} g_0 v \, ds. \quad (4)$$

We are interested in controlling the energy norm of the defeaturing error, which we suitably define in what follows.

*Negative feature case:* since  $\Omega \subset \Omega_0$  in this case, consider the restriction of  $u_0$  to  $\Omega$ . Then we define the defeaturing error as  $|u - u_0|_{1,\Omega}$ .

*Positive feature case:*  $u_0$  is not defined everywhere on  $\Omega$  since  $\Omega_0 \subset \Omega$  in this case. Therefore, to define the defeaturing error, one needs to solve an extension problem on  $F$ . The most natural extension would be the solution of

$$\begin{cases} -\Delta \tilde{u}_0 = f & \text{in } F \\ \tilde{u}_0 = u_0 & \text{on } \gamma_0 \\ \frac{\partial \tilde{u}_0}{\partial \mathbf{n}_F} = g & \text{on } \gamma. \end{cases} \quad (5)$$

However,  $F$  may be complex or even non-smooth (see Figure 14), thus the solution of (5) may be cumbersome. Therefore, let  $\tilde{F} \subset \mathbb{R}^n$  be an extended Lipschitz domain that contains  $F$  and such that  $\gamma_0 \subset (\partial \tilde{F} \cap \partial F)$ . Note that it is possible to have  $\tilde{F} \cap \Omega_0 \neq \emptyset$ , but we also assume that  $\tilde{F} \setminus F$  is Lipschitz. Thus if we consider any  $L^2$ -extension of  $f$  in  $\Omega \cup \tilde{F}$ , that we still write  $f \in L^2(\Omega \cup \tilde{F})$  by abuse of notation, then we can solve an extension problem in  $\tilde{F}$  instead of  $F$ .

This is illustrated in Figure 3: instead of solving the extension problem (5) in the feature  $F$ , we can choose to solve an extension problem in  $\tilde{F}$ , the bounding box of  $F$ , which shares  $\gamma_0$  as a boundary. Let

$\tilde{\gamma} := \partial\tilde{F} \setminus \partial F$  and let  $\mathbf{n}_{\tilde{F}}$  be the unitary outward normal of  $\tilde{F}$ . Note that  $\gamma_0$  and  $\tilde{\gamma}$  are “simple” boundaries since they are the boundaries of the chosen simplified geometry  $\Omega_0$  and of the chosen extended feature domain  $\tilde{F}$ , respectively.

Therefore, let us consider the following Dirichlet extension problem of (3) on  $\tilde{F}$ : given  $\tilde{g} \in H^{\frac{1}{2}}(\tilde{\gamma})$ , find  $\tilde{u}_0 \in H^1(\tilde{F})$ , the weak solution of

$$\begin{cases} -\Delta \tilde{u}_0 = f & \text{in } \tilde{F} \\ \tilde{u}_0 = u_0 & \text{on } \gamma_0 \\ \frac{\partial \tilde{u}_0}{\partial \mathbf{n}_{\tilde{F}}} = \tilde{g} & \text{on } \tilde{\gamma} \\ \frac{\partial \tilde{u}_0}{\partial \mathbf{n}_{\tilde{F}}} = g & \text{on } \gamma \cap \partial\tilde{F}, \end{cases} \quad (6)$$

that is  $\tilde{u}_0 \in H_{u_0, \gamma_0}^1(\tilde{F})$  satisfies for all  $v \in H_{0, \gamma_0}^1(\tilde{F})$ ,

$$\int_{\tilde{F}} \nabla \tilde{u}_0 \cdot \nabla v \, dx = \int_{\tilde{F}} f v \, dx + \int_{\tilde{\gamma}} \tilde{g} v \, ds + \int_{\gamma \cap \partial\tilde{F}} g v \, ds. \quad (7)$$

Let  $u_d \in H_{h, \Gamma_D}^1(\Omega)$  be the extended defeatured solution, that is

$$u_d = u_0 \text{ in } \Omega_0 \quad \text{and} \quad u_d = \tilde{u}_0|_F \text{ in } F. \quad (8)$$

Then we define the defeaturing error as  $|u - u_d|_{1, \Omega}$ .

In the remaining part of the article, the symbol  $\lesssim$  will be used to mean any inequality which does not depend on the size of the features  $F$  or  $\tilde{F}$  nor on their number, but it can depend on their shape. Moreover, we will need the following assumptions on different domains, so let  $\omega$  be any open  $k$ -dimensional manifold in  $\mathbb{R}^n$ ,  $k \leq n$ , not necessarily connected.

**Definition 3.1** We say that  $\omega$  is *isotropic* if each connected component  $\tilde{\omega}$  of  $\omega$  is isotropic, that is if  $\text{diam}(\tilde{\omega})^k \lesssim |\tilde{\omega}|$ , and if  $\text{diam}(\text{hull}(\omega)) \lesssim \max_{\tilde{\omega} \in \tilde{\Omega}} (\text{diam}(\tilde{\omega}))$ , where  $\tilde{\Omega}$  is the set of connected components of  $\omega$ .

**Definition 3.2** We say that  $\omega$  is *regular* if  $\omega$  is piecewise smooth and shape regular, that is if there is  $L_\omega \in \mathbb{N}$  such that  $\omega = \text{int} \left( \bigcup_{\ell=1}^{L_\omega} \overline{\omega_\ell} \right)$ ,  $\omega_\ell \cap \omega_k = \emptyset$ ,  $|\omega| \lesssim |\omega_\ell|$  and  $\omega_\ell$  is smooth, for all  $\ell, k = 1, \dots, L_\omega$ .

In particular, when a negative feature is considered, we suppose that  $\gamma$  is isotropic according to Definition 3.1, where the diameter and the convex hull of  $\gamma$  are considered in the manifold  $\partial\Omega$ . When a positive feature is considered, we suppose that  $\gamma_0$  and  $\gamma_\setminus := \gamma \setminus \partial\tilde{F}$  are isotropic, where the diameter and the convex hull of  $\gamma_0$  are considered in the manifold  $\partial\Omega_0$ , and the diameter and the convex hull of  $\gamma_\setminus$  are considered in the manifold  $\partial F$ . Note that in both cases, the considered boundaries can be non-connected sub-manifolds.

**Remark 3.3** The problem is studied in the case in which all domains are Lipschitz, and under the isotropy conditions stated above. A finer analysis could be performed to take into account more general geometries, such as the non-Lipschitz fillet of Figure 14, but this goes beyond the scope of this paper.

## 4 A posteriori defeaturing error estimator

In this section, an optimal a posteriori defeaturing error estimator is derived, first in the case of a positive feature, then in the case of a negative feature, and finally in the multi-feature case. We show that the derived estimator is both an upper bound and a lower bound up to oscillations, of the energy norm of the defeaturing error.

## 4.1 Negative feature a posteriori error estimator

Let  $F$  be a negative feature of  $\Omega$ , and suppose that  $\gamma$  is isotropic according to Definition 3.1. We define the defeaturing error estimator as

$$\mathcal{E}_n(u_0) := |\gamma|^{\frac{1}{2(n-1)}} \left\| g + \frac{\partial u_0}{\partial \mathbf{n}_F} \right\|_{0,\gamma}. \quad (9)$$

In this section, we show that under the compatibility condition (10) on the Neumann data  $g_0$ , the following holds:

$$|u - u_0|_{1,\Omega} \lesssim \mathcal{E}_n(u_0).$$

Moreover, assume that  $\gamma$  is also regular according to Definition 3.2. Then we also show that

$$\mathcal{E}_n(u_0) \lesssim |u - u_0|_{1,\Omega} + \text{osc}_n(u_0),$$

where  $\text{osc}_n(u_0)$  are oscillations defined in (16).

That is, we show that the quantity  $\mathcal{E}_n(u_0)$  is an estimator for the defeaturing error that is both reliable (see Theorem 4.1) and efficient up to oscillations (see Theorem 4.4). This means that the whole information on the error introduced by defeaturing a negative feature, in energy norm, is contained in the boundary  $\gamma$ , and can be accounted by suitably evaluating the error made on the normal derivative of the solution.

### 4.1.1 Upper bound

In this section, we prove that the error indicator defined in (9) is reliable, that is it is an upper bound for the defeaturing error.

**Theorem 4.1** *Let  $u$  and  $u_0$  be the weak solutions of problems (1) and (3), respectively. Let  $g_0 \in H^{\frac{1}{2}}(\gamma_0)$  such that*

$$\int_{\gamma_0} g_0 \, ds = \int_{\gamma} g \, ds - \int_F f \, dx. \quad (10)$$

*If  $\gamma$  is isotropic according to Definition 3.1, then the defeaturing error in energy norm is bounded in terms of the estimator  $\mathcal{E}_n(u_0)$  introduced in (9) as follows:*

$$|u - u_0|_{1,\Omega} \lesssim \mathcal{E}_n(u_0).$$

*Proof.* Let us first consider the simplified problem (3) restricted to  $\Omega$  with the natural Neumann boundary condition on  $\gamma$ , that is, since  $\mathbf{n}_F = -\mathbf{n}$  on  $\gamma$ ,  $u_0|_{\Omega} \in H_{h,\Gamma_D}^1(\Omega)$  is the weak solution of

$$\begin{cases} -\Delta(u_0|_{\Omega}) = f & \text{in } \Omega \\ u_0|_{\Omega} = h & \text{on } \Gamma_D \\ \frac{\partial(u_0|_{\Omega})}{\partial \mathbf{n}} = g & \text{on } \Gamma_N \setminus \gamma \\ \frac{\partial(u_0|_{\Omega})}{\partial \mathbf{n}} = -\frac{\partial u_0}{\partial \mathbf{n}_F} & \text{on } \gamma. \end{cases} \quad (11)$$

By abuse of notation, we omit the explicit restriction of  $u_0$  to  $\Omega$ . Then, for all  $v \in H_{0,\Gamma_D}^1(\Omega)$ ,

$$\int_{\Omega} \nabla u_0 \cdot \nabla v \, dx = \int_{\Omega} f v \, dx + \int_{\Gamma_N \setminus \gamma} g v \, ds - \int_{\gamma} \frac{\partial u_0}{\partial \mathbf{n}_F} v \, ds. \quad (12)$$

Let  $e := u - u_0 \in H_{0,\Gamma_D}^1(\Omega)$ . Then, from equations (2) and (12), for all  $v \in H_{0,\Gamma_D}^1(\Omega)$ , it holds that

$$\int_{\Omega} \nabla e \cdot \nabla v \, dx = \int_{\Gamma_N} g v \, ds - \int_{\Gamma_N \setminus \gamma} g v \, ds + \int_{\gamma} \frac{\partial u_0}{\partial \mathbf{n}_F} v \, ds = \int_{\gamma} \left( g + \frac{\partial u_0}{\partial \mathbf{n}_F} \right) v \, ds. \quad (13)$$

Now, consider the simplified problem (3) restricted to  $F$  with the natural Neumann boundary condition on  $\gamma$ , in a similar way to (11). By abuse of notation and as previously, we omit the explicit restriction of  $u_0$  to  $F$ . If we multiply the restricted problem by the constant function 1 and integrate by parts, then thanks to property (10),

$$0 = \int_F f \, dx + \int_{\gamma_0} g_0 \, ds + \int_{\gamma} \frac{\partial u_0}{\partial \mathbf{n}_F} \, ds = \int_{\gamma} \left( g + \frac{\partial u_0}{\partial \mathbf{n}_F} \right) \, ds. \quad (14)$$

So  $g + \frac{\partial u_0}{\partial \mathbf{n}_F}$  has zero average over  $\gamma$ . And thus if we take  $v = e \in H_{0,\Gamma_D}^1(\Omega)$  in (13), and if we write

$$\bar{e} := \frac{1}{|\gamma|} \int_{\gamma} e \, ds$$

the average of  $e$  over  $\gamma$ , then thanks to Poincaré inequality of Lemma A.1, and to the trace inequality,

$$\begin{aligned} |e|_{1,\Omega}^2 &= \int_{\gamma} \left( g + \frac{\partial u_0}{\partial \mathbf{n}_F} \right) e \, ds = \int_{\gamma} \left( g + \frac{\partial u_0}{\partial \mathbf{n}_F} \right) (e - \bar{e}) \, ds \leq \left\| g + \frac{\partial u_0}{\partial \mathbf{n}_F} \right\|_{0,\gamma} \|e - \bar{e}\|_{0,\gamma} \\ &\lesssim \left\| g + \frac{\partial u_0}{\partial \mathbf{n}_F} \right\|_{0,\gamma} |\gamma|^{\frac{1}{2(n-1)}} |e|_{\frac{1}{2},\gamma} \leq |\gamma|^{\frac{1}{2(n-1)}} \left\| g + \frac{\partial u_0}{\partial \mathbf{n}_F} \right\|_{0,\gamma} |e|_{\frac{1}{2},\partial\Omega} \\ &\lesssim |\gamma|^{\frac{1}{2(n-1)}} \left\| g + \frac{\partial u_0}{\partial \mathbf{n}_F} \right\|_{0,\gamma} |e|_{1,\Omega}. \end{aligned} \quad (15)$$

Therefore, by simplifying on both sides, we obtain the desired result.  $\square$

**Remark 4.2** The way to choose  $g_0$  as in equation (10) is desirable since this corresponds to the conservation of the solution flux across  $\gamma_0$  and  $\gamma$ . Indeed, if  $\frac{\partial u_0}{\partial \mathbf{n}_F} = -g$  on  $\gamma$ , then it is easy to see that  $u_0 = u$  in  $\Omega$  by uniqueness of the weak solution. In this case, if we look at (3) restricted to  $F$  with  $\frac{\partial u_0}{\partial \mathbf{n}_F} = -g$  on  $\gamma$ , if we multiply it by the constant function 1 and integrate by parts, then we find again property (10) as a necessary condition.

**Remark 4.3** If the feature is internal, that is if  $\gamma_0 = \emptyset$ , then (10) is a condition on the  $L^2$ -extension of  $f$  in  $F$  when defining the defeatured problem (3).

#### 4.1.2 Lower bound

In this section, we prove that the error indicator defined in (9) is efficient, that is it is a lower bound for the defeaturing error, up to oscillations.

Let  $\mathbf{m} \in \mathbb{N}^n$ , and if  $\gamma$  is regular, let  $\Pi_{\mathbf{m}} : H_0^{\frac{1}{2}}(\gamma) \rightarrow \mathbb{Q}_{\mathbf{m},0}^{\text{pw}}(\gamma)$  be the extension of the Clément operator [42] developed in [43]. By abuse of notation, we still write  $\Pi_{\mathbf{m}}$  instead of  $\Pi_{\mathbf{m}}|_{\gamma_\ell}$ , its restriction to any smooth subdomain  $\gamma_\ell$  of  $\gamma$ ,  $\ell = 1, \dots, L_\gamma$ .

**Theorem 4.4** *Let  $u, u_0, g_0$  and  $f$  be as in Theorem 4.1, and assume that  $\gamma$  is isotropic and regular according to Definitions 3.1 and 3.2. Then the defeaturing error, in energy norm, bounds up to oscillations the estimator  $\mathcal{E}_n(u_0)$  introduced in (9), that is*

$$\mathcal{E}_n(u_0) \lesssim |u - u_0|_{1,\Omega} + \text{osc}_n(u_0),$$

where

$$\begin{aligned} \text{osc}_n(u_0) &:= \left( \sum_{\ell=1}^{L_\gamma} \text{osc}_{n,\ell}(u_0)^2 \right)^{\frac{1}{2}}, \\ \text{osc}_{n,\ell}(u_0) &:= |\gamma|^{\frac{1}{2(n-1)}} \left\| \left( g + \frac{\partial u_0}{\partial \mathbf{n}_F} \right) - \Pi_{\mathbf{m}} \left( g + \frac{\partial u_0}{\partial \mathbf{n}_F} \right) \right\|_{0,\gamma_\ell}, \quad \forall \ell = 1, \dots, L_\gamma. \end{aligned} \quad (16)$$



*Proof.* To simplify the notation, we omit to explicitly write the restriction of  $u_0$  to  $\Omega$  when it would be necessary, since the context makes it clear. Let  $e := u - u_0 \in H_{0,\Gamma_D}^1(\Omega)$ . From equation (13), for all  $v \in H_{0,\Gamma_D}^1(\Omega)$ ,

$$\int_{\gamma} \left( g + \frac{\partial u_0}{\partial \mathbf{n}_F} \right) v \, ds = \int_{\Omega} \nabla e \cdot \nabla v \, dx \leq |e|_{1,\Omega} |v|_{1,\Omega}.$$

Now, for all  $w \in H_{00}^{\frac{1}{2}}(\gamma)$ , let  $u_w \in H_{0,\partial\Omega \setminus \gamma}^1(\Omega) \subset H_{0,\Gamma_D}^1(\Omega)$  be the unique weak solution of

$$\begin{cases} -\Delta u_w = 0 & \text{in } \Omega \\ u_w = w^* & \text{on } \partial\Omega, \end{cases}$$

where  $w^*$  is the extension of  $w$  by 0. Then  $|u_w|_{1,\Omega} \lesssim \|w^*\|_{\frac{1}{2},\partial\Omega} = \|w\|_{\frac{1}{2},\gamma} \lesssim \|w\|_{H_{00}^{1/2}(\gamma)}$  by continuity of the solution on the data. Therefore,

$$\begin{aligned} \left\| g + \frac{\partial u_0}{\partial \mathbf{n}_F} \right\|_{H_{00}^{-1/2}(\gamma)} &= \sup_{\substack{w \in H_{00}^{1/2}(\gamma) \\ w \neq 0}} \frac{\int_{\gamma} \left( g + \frac{\partial u_0}{\partial \mathbf{n}_F} \right) w \, ds}{\|w\|_{H_{00}^{1/2}(\gamma)}} \lesssim \sup_{\substack{w \in H_{00}^{1/2}(\gamma) \\ w \neq 0}} \frac{\int_{\gamma} \left( g + \frac{\partial u_0}{\partial \mathbf{n}_F} \right) u_w \, ds}{|u_w|_{1,\Omega}} \\ &\leq \sup_{\substack{v \in H_{0,\Gamma_D}^1(\Omega) \\ v \neq 0}} \frac{\int_{\gamma} \left( g + \frac{\partial u_0}{\partial \mathbf{n}_F} \right) v \, ds}{|v|_{1,\Omega}} \leq \sup_{\substack{v \in H_{0,\Gamma_D}^1(\Omega) \\ v \neq 0}} \frac{|e|_{1,\Omega} |v|_{1,\Omega}}{|v|_{1,\Omega}} = |e|_{1,\Omega}. \end{aligned} \quad (17)$$

Then, thanks to Lemmas A.3 and A.4,

$$\begin{aligned} &|\gamma|^{\frac{1}{2(n-1)}} \left\| g + \frac{\partial u_0}{\partial \mathbf{n}_F} \right\|_{0,\gamma} \\ &\leq |\gamma|^{\frac{1}{2(n-1)}} \left\| \Pi_{\mathbf{m}} \left( g + \frac{\partial u_0}{\partial \mathbf{n}_F} \right) \right\|_{0,\gamma} + |\gamma|^{\frac{1}{2(n-1)}} \left\| \left( g + \frac{\partial u_0}{\partial \mathbf{n}_F} \right) - \Pi_{\mathbf{m}} \left( g + \frac{\partial u_0}{\partial \mathbf{n}_F} \right) \right\|_{0,\gamma} \\ &\lesssim \left\| \Pi_{\mathbf{m}} \left( g + \frac{\partial u_0}{\partial \mathbf{n}_F} \right) \right\|_{H_{00}^{-1/2}(\gamma)} + \text{osc}_{\mathbf{n}}(u_0) \\ &\leq \left\| g + \frac{\partial u_0}{\partial \mathbf{n}_F} \right\|_{H_{00}^{-1/2}(\gamma)} + \left\| \Pi_{\mathbf{m}} \left( g + \frac{\partial u_0}{\partial \mathbf{n}_F} \right) - \left( g + \frac{\partial u_0}{\partial \mathbf{n}_F} \right) \right\|_{H_{00}^{-1/2}(\gamma)} + \text{osc}_{\mathbf{n}}(u_0) \\ &\lesssim \left\| g + \frac{\partial u_0}{\partial \mathbf{n}_F} \right\|_{H_{00}^{-1/2}(\gamma)} + \text{osc}_{\mathbf{n}}(u_0), \end{aligned} \quad (18)$$

Consequently, from (17) and (18),

$$\mathcal{E}_{\mathbf{n}}(u_0) = |\gamma|^{\frac{1}{2(n-1)}} \left\| g + \frac{\partial u_0}{\partial \mathbf{n}_F} \right\|_{0,\gamma} \lesssim \left\| g + \frac{\partial u_0}{\partial \mathbf{n}_F} \right\|_{H_{00}^{-1/2}(\gamma)} + \text{osc}_{\mathbf{n}}(u_0) \lesssim |e|_{1,\Omega} + \text{osc}_{\mathbf{n}}(u_0).$$

□

**Remark 4.5** In some sense, the oscillations pollute the lower bound in Theorem 4.4. It is therefore important to make sure that the oscillations are asymptotically smaller than the defeaturing error, with respect to the size of the feature. While there is a strong numerical evidence of it (see Section 5), an a priori error analysis of the defeaturing problem is needed in order to obtain a rigorous proof. However, we are expecting the term  $\left\| g + \frac{\partial u_0}{\partial \mathbf{n}_F} \right\|_{0,\gamma}$  to depend on the measure of  $\gamma$ . When the data is regular, so is  $u_0$ , and it is then always possible to choose  $\mathbf{m} = (m, \dots, m)$  with  $m$  large enough so that the asymptotic behavior of the oscillations is  $\mathcal{O}\left(|\gamma|^{m+\frac{1}{2(n-1)}}\right)$ . Therefore, upon a wise choice of  $\mathbf{m}$ , the oscillations converge faster than the defeaturing error with respect to the measure of  $\gamma$ .

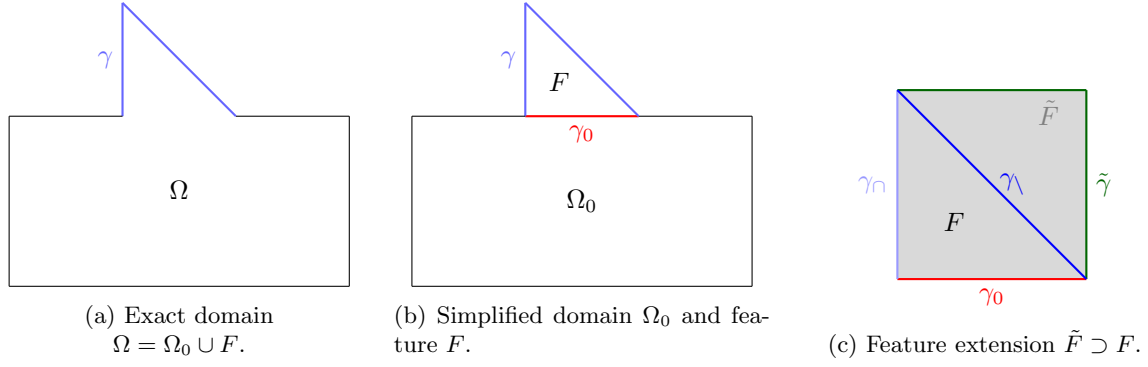


Figure 4: Illustration of the boundaries notation on an example.

## 4.2 Positive feature a posteriori error estimator

Suppose that  $F$  is a positive feature of  $\Omega$ , and let us use the notation introduced in Section 3, with  $F \subset \tilde{F} \subset \mathbb{R}^n$  such that  $\gamma_0 \subset (\partial\tilde{F} \cap \partial F)$ . Moreover, let  $\gamma = \text{int}(\overline{\gamma_\cap} \cup \overline{\gamma_\backslash})$ , where  $\gamma_\cap$  and  $\gamma_\backslash$  are open,  $\gamma_\cap$  is the part of  $\gamma$  that also belongs to  $\partial\tilde{F}$ , while  $\gamma_\backslash$  is the part of  $\gamma$  that does not belong to  $\partial\tilde{F}$ . This notation is illustrated on an example in Figure 4. Finally, suppose that  $\gamma_0$  and  $\gamma_\backslash$  are isotropic according to Definition 3.1.

Let us define the defeaturing error estimator as

$$\mathcal{E}_p(\tilde{u}_0) := \left( |\gamma_0|^{\frac{1}{n-1}} \left\| g_0 + \frac{\partial \tilde{u}_0}{\partial \mathbf{n}_F} \right\|_{0, \gamma_0}^2 + |\gamma_\backslash|^{\frac{1}{n-1}} \left\| g - \frac{\partial \tilde{u}_0}{\partial \mathbf{n}_F} \right\|_{0, \gamma_\backslash}^2 \right)^{\frac{1}{2}}. \quad (19)$$

In this section, we show that under the compatibility conditions (20) and (21) on the Neumann data  $g_0$  and  $\tilde{g}$ , the following holds:

$$|u - u_d|_{1, \Omega} \lesssim \mathcal{E}_p(\tilde{u}_0).$$

Moreover, assume that  $\gamma_0$  and  $\gamma_\backslash$  are also regular according to Definition 3.2. Then we also show that

$$\mathcal{E}_p(\tilde{u}_0) \lesssim |u - u_d|_{1, \Omega} + \text{osc}_p(\tilde{u}_0),$$

where  $\text{osc}_p(\tilde{u}_0)$  are oscillations defined in (32).

That is, we show that the quantity  $\mathcal{E}_p(\tilde{u}_0)$  defined in (19) is an estimator for the defeaturing error that is both reliable (see Theorem 4.6) and efficient up to oscillations (see Theorem 4.8). This means that all the information on the error introduced by defeaturing a positive feature, in energy norm, is contained in the boundary of  $F$ , and can be accounted by suitably evaluating the error made on the normal derivative of the solution.

### 4.2.1 Upper bound

In this section, we prove that the error indicator defined in (19) is reliable, that is it is an upper bound for the defeaturing error.

**Theorem 4.6** *Let  $u$ ,  $u_0$  and  $\tilde{u}_0$  be the weak solutions of problems (1), (3) and (6) respectively, and let  $u_d \in H_{0, \Gamma_D}^1(\Omega)$  be as defined in (8). Let  $g_0 \in H^{\frac{1}{2}}(\gamma_0)$  such that*

$$\int_{\gamma_0} g_0 \, ds = \int_{\gamma} g \, ds + \int_F f \, dx, \quad (20)$$

*and finally, let  $\tilde{g} \in H^{\frac{1}{2}}(\tilde{\gamma})$  such that*

$$\int_{\tilde{\gamma}} \tilde{g} \, ds = \int_{\gamma_\backslash} g \, ds - \int_{\tilde{F} \setminus F} f \, dx. \quad (21)$$

If  $\gamma_0$  and  $\gamma_\backslash$  are isotropic according to Definition 3.1, then the defeating error in energy norm is bounded in terms of the estimator  $\mathcal{E}_p(\tilde{u}_0)$  introduced in (19) as follows:

$$|u - u_d|_{1,\Omega} \lesssim \mathcal{E}_p(\tilde{u}_0).$$

*Proof.* The proof is very similar to the one of Theorem 4.1. Let us first consider the original problem (1) restricted to  $\Omega_0$  with the natural Neumann boundary condition on  $\gamma_0$ , that is  $u|_{\Omega_0} \in H_{h,\Gamma_D}^1(\Omega_0)$  is the weak solution of

$$\begin{cases} -\Delta(u|_{\Omega_0}) = f & \text{in } \Omega_0 \\ u|_{\Omega_0} = h & \text{on } \Gamma_D \\ \frac{\partial(u|_{\Omega_0})}{\partial \mathbf{n}_0} = g & \text{on } \Gamma_N \setminus \gamma \\ \frac{\partial(u|_{\Omega_0})}{\partial \mathbf{n}_0} = \frac{\partial u}{\partial \mathbf{n}_0} & \text{on } \gamma_0, \end{cases} \quad (22)$$

By abuse of notation, we omit the explicit restriction of  $u$  to  $\Omega_0$ . Then for all  $v_0 \in H_{0,\Gamma_D}^1(\Omega_0)$ ,

$$\int_{\Omega_0} \nabla u \cdot \nabla v_0 \, dx = \int_{\Omega_0} f v_0 \, dx + \int_{\Gamma_N \setminus \gamma} g v_0 \, ds + \int_{\gamma_0} \frac{\partial u}{\partial \mathbf{n}_0} v_0 \, ds. \quad (23)$$

Let  $e := u - u_d$ . Then from the weak simplified problem (4) and from (23), for all  $v_0 \in H_{0,\Gamma_D}^1(\Omega_0)$ ,

$$\int_{\Omega_0} \nabla e \cdot \nabla v_0 \, dx = \int_{\gamma_0} \left( \frac{\partial u}{\partial \mathbf{n}_0} - g_0 \right) v_0 \, ds. \quad (24)$$

Now, let us consider the simplified extended problem (6) restricted to  $F$  with the natural Neumann boundary condition on  $\gamma_\backslash$ , in a similar way to (22). By abuse of notation and as previously, we omit the explicit restriction of  $\tilde{u}_0$  to  $F$ . That is,  $\tilde{u}_0 \in H^1(F)$  is one of the infinitely-many solutions (up to a constant) of

$$\int_F \nabla \tilde{u}_0 \cdot \nabla \tilde{v} \, dx = \int_F f \tilde{v} \, dx + \int_{\gamma_\cap} g \tilde{v} \, ds + \int_{\gamma_0 \cup \gamma_\backslash} \frac{\partial \tilde{u}_0}{\partial \mathbf{n}_F} \tilde{v} \, ds, \quad \forall \tilde{v} \in H^1(F), \quad (25)$$

And let us consider the original problem (1) restricted to  $F$  with the natural Neumann boundary condition on  $\gamma_0$ , again in a similar way to (22). By abuse of notation and as previously, we omit the explicit restriction of  $u$  to  $F$ . So  $u \in H^1(F)$  is one of the infinitely-many solutions (up to a constant) of

$$\int_F \nabla u \cdot \nabla \tilde{v} \, dx = \int_F f \tilde{v} \, dx + \int_\gamma g \tilde{v} \, ds + \int_{\gamma_0} \frac{\partial u}{\partial \mathbf{n}_F} \tilde{v} \, ds, \quad \forall \tilde{v} \in H^1(F). \quad (26)$$

Consequently, from (25) and (26), for all  $\tilde{v} \in H^1(F)$ ,

$$\int_F \nabla e \cdot \nabla \tilde{v} \, dx = \int_{\gamma_0} \frac{\partial(u - \tilde{u}_0)}{\partial \mathbf{n}_F} \tilde{v} \, ds + \int_{\gamma_\backslash} \left( g - \frac{\partial \tilde{u}_0}{\partial \mathbf{n}_F} \right) \tilde{v} \, ds. \quad (27)$$

Let  $v \in H_{0,\Gamma_D}^1(\Omega)$ , then  $v|_{\Omega_0} \in H_{0,\Gamma_D}^1(\Omega_0)$  and  $v|_F \in H^1(F)$ . Therefore, from equations (24) and (27), since  $\mathbf{n}_0 = -\mathbf{n}_F$  on  $\gamma_0$ , we can deduce that

$$\int_\Omega \nabla e \cdot \nabla v \, dx = - \int_{\gamma_0} \left( g_0 + \frac{\partial \tilde{u}_0}{\partial \mathbf{n}_F} \right) v \, ds + \int_{\gamma_\backslash} \left( g - \frac{\partial \tilde{u}_0}{\partial \mathbf{n}_F} \right) v \, ds. \quad (28)$$

Furthermore, consider the simplified problem (6) restricted to  $\tilde{F} \setminus F$  with the natural Neumann boundary condition on  $\gamma_\backslash$ , again in a similar way to (22). By abuse of notation and as previously, we omit the explicit restriction of  $\tilde{u}_0$  to  $\tilde{F} \setminus F$ . If we test the restricted problem against a constant function, we get

$$\int_{\gamma_\backslash} \frac{\partial \tilde{u}_0}{\partial \mathbf{n}_F} \, ds = \int_{\tilde{F} \setminus F} f \, dx + \int_{\tilde{\gamma}} \tilde{g} \, ds = \int_{\gamma_\backslash} g \, ds. \quad (29)$$

Moreover, by taking  $v \equiv 1$  in equation (25), and thanks to (20) and (29), then

$$-\int_{\gamma_0} \frac{\partial \tilde{u}_0}{\partial \mathbf{n}_F} ds = \int_F f dx + \int_{\gamma_0} g ds + \int_{\gamma_\lambda} \frac{\partial \tilde{u}_0}{\partial \mathbf{n}_F} ds = \int_F f dx + \int_{\gamma} g ds = \int_{\gamma_0} g_0 ds. \quad (30)$$

Consequently, from equations (29) and (30), we deduce that  $g - \frac{\partial \tilde{u}_0}{\partial \mathbf{n}_F}$  has zero average over  $\gamma_\lambda$ , and that  $g_0 + \frac{\partial \tilde{u}_0}{\partial \mathbf{n}_F}$  has zero average over  $\gamma_0$ . Therefore, by taking  $v = e \in H_{0,\Gamma_D}^1(\Omega)$  in (28), writing

$$\bar{e}^{\gamma_0} := \frac{1}{|\gamma_0|} \int_{\gamma_0} e ds \quad \text{and} \quad \bar{e}^{\gamma_\lambda} := \frac{1}{|\gamma_\lambda|} \int_{\gamma_\lambda} e ds,$$

and following the same steps as for the proof of Theorem 4.1, using Lemma A.1, we obtain

$$\begin{aligned} |e|_{1,\Omega}^2 &= - \int_{\gamma_0} \left( g_0 + \frac{\partial \tilde{u}_0}{\partial \mathbf{n}_F} \right) e ds + \int_{\gamma_\lambda} \left( g - \frac{\partial \tilde{u}_0}{\partial \mathbf{n}_F} \right) e ds \\ &= - \int_{\gamma_0} \left( g_0 + \frac{\partial \tilde{u}_0}{\partial \mathbf{n}_F} \right) (e - \bar{e}^{\gamma_0}) ds + \int_{\gamma_\lambda} \left( g - \frac{\partial \tilde{u}_0}{\partial \mathbf{n}_F} \right) (e - \bar{e}^{\gamma_\lambda}) ds \\ &\lesssim |\gamma_0|^{\frac{1}{2(n-1)}} \left\| g_0 + \frac{\partial \tilde{u}_0}{\partial \mathbf{n}_F} \right\|_{0,\gamma_0} |e|_{\frac{1}{2},\gamma_0} + |\gamma_\lambda|^{\frac{1}{2(n-1)}} \left\| g - \frac{\partial \tilde{u}_0}{\partial \mathbf{n}_F} \right\|_{0,\gamma_\lambda} |e|_{\frac{1}{2},\gamma_\lambda} \\ &\lesssim \left( |\gamma_0|^{\frac{1}{n-1}} \left\| g_0 + \frac{\partial \tilde{u}_0}{\partial \mathbf{n}_F} \right\|_{0,\gamma_0}^2 + |\gamma_\lambda|^{\frac{1}{n-1}} \left\| g - \frac{\partial \tilde{u}_0}{\partial \mathbf{n}_F} \right\|_{0,\gamma_\lambda}^2 \right)^{\frac{1}{2}} |e|_{1,\Omega}, \end{aligned} \quad (31)$$

where the discrete Cauchy-Schwarz inequality is used to obtain (31). Therefore, by simplifying on both sides, and from the definition (19) of  $\mathcal{E}_p(\tilde{u}_0)$ , we obtain the desired result.  $\square$

**Remark 4.7** The way to choose  $g_0$  as in equation (20) and  $\tilde{g}$  as in equation (21) is natural and desirable since this corresponds to the conservation of the solution flux across the boundaries of  $F$  and  $\tilde{F}$ .

#### 4.2.2 Lower bound

In this section, we prove that the error indicator defined in (19) is efficient, that is it is a lower bound for the defeating error, up to oscillations.

Let  $\mathbf{m} \in \mathbb{N}^n$ . To simplify the notation when  $\gamma_0$  and  $\gamma_\lambda$  are regular, let us write  $L_0 := L_{\gamma_0}$  and  $L_1 := L_{\gamma_\lambda}$ . Then let  $\Pi_{0\mathbf{m}} : H_0^{\frac{1}{2}}(\gamma_0) \rightarrow \mathbb{Q}_{\mathbf{m},0}^{\text{pw}}(\gamma_0)$  and  $\Pi_{\lambda\mathbf{m}} : H_0^{\frac{1}{2}}(\gamma_\lambda) \rightarrow \mathbb{Q}_{\mathbf{m},0}^{\text{pw}}(\gamma_\lambda)$  be the extensions of the Clément operator [42] developed in [43], and let us define  $\Pi_{\mathbf{m}}$  such that  $\Pi_{\mathbf{m}}|_{\gamma_0} \equiv \Pi_{0\mathbf{m}}$  and  $\Pi_{\mathbf{m}}|_{\gamma_\lambda} \equiv \Pi_{\lambda\mathbf{m}}$ . By abuse of notation, we still write  $\Pi_{\mathbf{m}}$  instead of its restriction to any smooth subdomain  $\gamma_{0\ell}$  of  $\gamma_0$ ,  $\ell = 1, \dots, L_0$ , or  $\gamma_{\lambda\ell}$  of  $\gamma_\lambda$ ,  $\ell = 1, \dots, L_1$ .

**Theorem 4.8** *Let  $u$ ,  $u_0$ ,  $\tilde{u}_0$ ,  $u_d$ ,  $g_0$  and  $\tilde{g}$  be as in Theorem 4.6, and assume that  $\gamma_0$  and  $\gamma_\lambda$  are isotropic and regular according to Definitions 3.1 and 3.2. Then the defeating error, in energy norm, bounds up to oscillations the estimator  $\mathcal{E}_p(\tilde{u}_0)$  introduced in (19), that is*

$$\mathcal{E}_p(\tilde{u}_0) \lesssim |u - u_d|_{1,\Omega} + \text{osc}_p(\tilde{u}_0),$$

where

$$\begin{aligned}
\text{osc}_{\mathbf{p}}(\tilde{u}_0) &:= |\gamma_0 \cup \gamma_\lambda|^{\frac{1}{2(n-1)}} \left( \sum_{\ell=1}^{L_0+L_1} \text{osc}_{\mathbf{p},\ell}(\tilde{u}_0)^2 \right)^{\frac{1}{2}}, \\
\text{osc}_{\mathbf{p},\ell}(\tilde{u}_0) &:= \left\| \left( g_0 + \frac{\partial \tilde{u}_0}{\partial \mathbf{n}_F} \right) - \Pi_{\mathbf{m}} \left( g_0 + \frac{\partial \tilde{u}_0}{\partial \mathbf{n}_F} \right) \right\|_{0,\gamma_{0\ell}}, \quad \forall \ell = 1, \dots, L_0, \\
\text{osc}_{\mathbf{p},L_0+\ell}(\tilde{u}_0) &:= \left\| \left( g - \frac{\partial \tilde{u}_0}{\partial \mathbf{n}_F} \right) - \Pi_{\mathbf{m}} \left( g - \frac{\partial \tilde{u}_0}{\partial \mathbf{n}_F} \right) \right\|_{0,\gamma_{\lambda\ell}}, \quad \forall \ell = 1, \dots, L_1.
\end{aligned} \tag{32}$$

*Proof.* The proof is similar to the one of Theorem 4.4. Let  $e := u - u_d \in H_{0,\Gamma_D}^1(\Omega)$ . From equations (24) and (27), for all  $v \in H^1(F)$  and all  $v_0 \in H_{0,\Gamma_D}^1(\Omega_0)$ ,

$$\int_{\gamma_0 \cup \gamma_\lambda} \frac{\partial(u - \tilde{u}_0)}{\partial \mathbf{n}_F} v \, ds = \int_{\gamma_0} \frac{\partial(u - \tilde{u}_0)}{\partial \mathbf{n}_F} v \, ds + \int_{\gamma_\lambda} \left( g - \frac{\partial \tilde{u}_0}{\partial \mathbf{n}_F} \right) v \, ds = \int_F \nabla e \cdot \nabla v \, dx \leq |e|_{1,F} |v|_{1,F}, \tag{33}$$

$$\int_{\gamma_0} \left( \frac{\partial u}{\partial \mathbf{n}_0} - g_0 \right) v_0 \, ds = \int_{\Omega_0} \nabla e \cdot \nabla v_0 \, dx \leq |e|_{1,\Omega_0} |v_0|_{1,\Omega_0}. \tag{34}$$

Now, for all  $w \in H_{00}^{\frac{1}{2}}(\gamma_0 \cup \gamma_\lambda)$ , let  $u_w \in H_{0,\gamma_\Gamma}^1(F) \subset H^1(F)$  be the unique weak solution of

$$\begin{cases} -\Delta u_w = 0 & \text{in } F \\ u_w = w^* & \text{on } \partial F. \end{cases}$$

Then  $|u_w|_{1,F} \lesssim \|w^*\|_{\frac{1}{2},\partial F} = \|w\|_{\frac{1}{2},\gamma_0 \cup \gamma_\lambda} \lesssim \|w\|_{H_{00}^{1/2}(\gamma_0 \cup \gamma_\lambda)}$  by continuity of the solution on the data. Therefore, thanks to (33),

$$\begin{aligned}
\left\| \frac{\partial(u - \tilde{u}_0)}{\partial \mathbf{n}_F} \right\|_{H_{00}^{-1/2}(\gamma_0 \cup \gamma_\lambda)} &= \sup_{\substack{w \in H_{00}^{1/2}(\gamma_0 \cup \gamma_\lambda) \\ w \neq 0}} \frac{\int_{\gamma_0 \cup \gamma_\lambda} \frac{\partial(u - \tilde{u}_0)}{\partial \mathbf{n}_F} w \, ds}{\|w\|_{H_{00}^{1/2}(\gamma_0 \cup \gamma_\lambda)}} \\
&\lesssim \sup_{\substack{w \in H_{00}^{1/2}(\gamma_0 \cup \gamma_\lambda) \\ w \neq 0}} \frac{\int_{\gamma_0 \cup \gamma_\lambda} \frac{\partial(u - \tilde{u}_0)}{\partial \mathbf{n}_F} u_w \, ds}{|u_w|_{1,F}} \leq \sup_{\substack{v \in H^1(F) \\ v \neq 0}} \frac{\int_{\gamma_0 \cup \gamma_\lambda} \frac{\partial(u - \tilde{u}_0)}{\partial \mathbf{n}_F} v \, ds}{|v|_{1,F}} \leq |e|_{1,F}.
\end{aligned} \tag{35}$$

In a completely analogous way, we can prove thanks to (34) that

$$\left\| \frac{\partial u}{\partial \mathbf{n}_0} - g_0 \right\|_{H_{00}^{-1/2}(\gamma_0)} \lesssim |e|_{1,\Omega_0}. \tag{36}$$

Then from (35) and (36),

$$\left( \left\| \frac{\partial(u - \tilde{u}_0)}{\partial \mathbf{n}_F} \right\|_{H_{00}^{-1/2}(\gamma_0 \cup \gamma_\lambda)}^2 + \left\| \frac{\partial u}{\partial \mathbf{n}_0} - g_0 \right\|_{H_{00}^{-1/2}(\gamma_0)}^2 \right)^{\frac{1}{2}} \lesssim (|e|_{1,F}^2 + |e|_{1,\Omega_0}^2)^{\frac{1}{2}} = |e|_{1,\Omega}. \tag{37}$$

From inequality (37), by linearity of the Clément operator, by exploiting its approximation properties, and

by the inverse inequality of Lemma A.3, we obtain

$$\begin{aligned}
\mathcal{E}_p(\tilde{u}_0)^2 &\lesssim |\gamma_0|^{\frac{1}{n-1}} \left\| g_0 + \frac{\partial u}{\partial \mathbf{n}_F} \right\|_{0,\gamma_0}^2 + |\gamma_0|^{\frac{1}{n-1}} \left\| \frac{\partial(u - \tilde{u}_0)}{\partial \mathbf{n}_F} \right\|_{0,\gamma_0}^2 + |\gamma_\backslash|^{\frac{1}{n-1}} \left\| \frac{\partial(u - \tilde{u}_0)}{\partial \mathbf{n}_F} \right\|_{0,\gamma_\backslash}^2 \\
&\lesssim \left\| g_0 + \frac{\partial u}{\partial \mathbf{n}_F} \right\|_{H_{00}^{-1/2}(\gamma_0)}^2 + \left\| \left( g_0 + \frac{\partial u}{\partial \mathbf{n}_F} \right) - \Pi_{\mathbf{m}} \left( g_0 + \frac{\partial u}{\partial \mathbf{n}_F} \right) \right\|_{H_{00}^{-1/2}(\gamma_0)}^2 \\
&\quad + \left\| \frac{\partial(u - \tilde{u}_0)}{\partial \mathbf{n}_F} \right\|_{H_{00}^{-1/2}(\gamma_0 \cup \gamma_\backslash)}^2 + \left\| \frac{\partial(u - \tilde{u}_0)}{\partial \mathbf{n}_F} - \Pi_{\mathbf{m}} \left( \frac{\partial(u - \tilde{u}_0)}{\partial \mathbf{n}_F} \right) \right\|_{H_{00}^{-1/2}(\gamma_0 \cup \gamma_\backslash)}^2 + \text{osc}_p(\tilde{u}_0)^2 \\
&\lesssim |e|_{1,\Omega}^2 + |\gamma_0|^{\frac{1}{n-1}} \left\| \left( g_0 + \frac{\partial u}{\partial \mathbf{n}_F} \right) - \Pi_{\mathbf{m}} \left( g_0 + \frac{\partial u}{\partial \mathbf{n}_F} \right) \right\|_{0,\gamma_0}^2 \\
&\quad + |\gamma_0 \cup \gamma_\backslash|^{\frac{1}{n-1}} \left\| \left( \frac{\partial(u - \tilde{u}_0)}{\partial \mathbf{n}_F} \right) - \Pi_{\mathbf{m}} \left( \frac{\partial(u - \tilde{u}_0)}{\partial \mathbf{n}_F} \right) \right\|_{0,\gamma_0 \cup \gamma_\backslash}^2 + \text{osc}_p(\tilde{u}_0)^2 \\
&\lesssim (|e|_{1,\Omega} + \text{osc}_p(\tilde{u}_0))^2,
\end{aligned} \tag{38}$$

where inequality (38) has been obtained thanks to Lemma A.4.  $\square$

**Remark 4.9** In some sense, the oscillations pollute the lower bound in Theorem 4.8. It is therefore important to make sure that the oscillations get small with respect to the defeaturing error, when the feature gets small. As in Remark 4.5, when the data is regular, it is always possible to choose  $\mathbf{m} = (m, \dots, m)$  with  $m$  large enough so that the asymptotic behavior of the oscillations is  $\mathcal{O}\left(\max(|\gamma_0|, |\gamma_\backslash|)^{m + \frac{1}{2(n-1)}}\right)$ .

### 4.3 Choosing the defeatured Neumann boundary conditions

One would like to choose the Neumann boundary conditions  $g_0$  and  $\tilde{g}$  of problems (3) and (6) such that the defeaturing error is minimized. But the error is unknown, and  $g_0$  and  $\tilde{g}$  are required to determine the defeatured solution  $u_d$ . Therefore, we have to choose them a priori, such that assumptions (10), (20) and (21) are satisfied.

The easiest choice is to take the following constant functions:

- if  $F$  is negative, let

$$g_0 := g_0^{(0)} \equiv \frac{1}{|\gamma_0|} \left( \int_{\gamma} g \, ds - \int_F f \, dx \right);$$

- if  $F$  is positive, let

$$g_0 := g_0^{(0)} \equiv \frac{1}{|\gamma_0|} \left( \int_{\gamma} g \, ds + \int_F f \, dx \right) \quad \text{and} \quad \tilde{g} := \tilde{g}^{(0)} \equiv \frac{1}{|\tilde{\gamma}|} \left( \int_{\gamma_\backslash} g \, ds - \int_{\tilde{F} \setminus F} f \, dx \right).$$

Another choice is to consider the quadratic functions  $g_0 := g_0^{(2)}$  and  $\tilde{g} := \tilde{g}^{(2)}$  such that:

- if  $F$  is negative, (10) is satisfied and  $g = g_0$  on  $\partial\gamma \cap \partial\gamma_0$ ;
- if  $F$  is positive, (20) and (21) are satisfied,  $g = g_0$  on  $\partial\gamma \cap \partial\gamma_0$ , and  $g = \tilde{g}$  on  $\partial\gamma_\backslash \cap \partial\tilde{\gamma}$ .

We use the superindex  $^{(i)}$  with  $i = 0, 2$  to denote quantities obtained with these two choices. In the following, we compare the errors  $e^{(0)}$  and  $e^{(2)}$  in the case of a negative feature, and we report the analogous result in

the case of a positive feature. The estimates (41) and (42) below, together with our numerical validation (discussed in Section 5) show that choosing  $g_0^{(0)}$  and  $\tilde{g}^{(0)}$  is good enough and guarantees the optimality of our defeaturing error indicator.

Suppose that  $F$  is a negative feature, as in Section 4.1. In the proof of Theorem 4.1, we have seen that

$$\left|e^{(2)}\right|_{1,\Omega}^2 = \int_{\gamma} \left(g + \frac{\partial u_0^{(2)}}{\partial \mathbf{n}_F}\right) e^{(2)} \, ds$$

and since  $g + \frac{\partial u_0^{(0)}}{\partial \mathbf{n}_F}$  has zero average on  $\gamma$ , by the exact same steps as in (15) in the proof of Theorem 4.1,

$$\int_{\gamma} \left(g + \frac{\partial u_0^{(0)}}{\partial \mathbf{n}_F}\right) e^{(2)} \, ds \lesssim |\gamma|^{\frac{1}{2(n-1)}} \left\|g + \frac{\partial u_0^{(0)}}{\partial \mathbf{n}_F}\right\|_{0,\gamma} \left|e^{(2)}\right|_{1,\Omega} = \mathcal{E}_n(u_0^{(0)}) \left|e^{(2)}\right|_{1,\Omega}.$$

Therefore,

$$\begin{aligned} \left|e^{(2)}\right|_{1,\Omega}^2 &= \int_{\gamma} \left(g + \frac{\partial u_0^{(0)}}{\partial \mathbf{n}_F}\right) e^{(2)} \, ds - \int_{\gamma} \left(\frac{\partial u_0^{(0)}}{\partial \mathbf{n}_F} - \frac{\partial u_0^{(2)}}{\partial \mathbf{n}_F}\right) e^{(2)} \, ds \\ &\lesssim \mathcal{E}_n(u_0^{(0)}) \left|e^{(2)}\right|_{1,\Omega} + \left\|\frac{\partial u_0^{(0)}}{\partial \mathbf{n}_F} - \frac{\partial u_0^{(2)}}{\partial \mathbf{n}_F}\right\|_{-\frac{1}{2},\gamma} \|e^{(2)}\|_{\frac{1}{2},\gamma}. \end{aligned} \quad (39)$$

Moreover, by trace inequality, and since  $g_0^{(0)}$  and  $g_0^{(2)}$  have the same average thanks to (10), then

$$\begin{aligned} \left\|\frac{\partial u_0^{(0)}}{\partial \mathbf{n}_F} - \frac{\partial u_0^{(2)}}{\partial \mathbf{n}_F}\right\|_{-\frac{1}{2},\gamma} \|e^{(2)}\|_{\frac{1}{2},\gamma} &\lesssim \left|u_0^{(0)} - u_0^{(2)}\right|_{1,\Omega} \left|e^{(2)}\right|_{1,\Omega} \lesssim \left|u_0^{(0)} - u_0^{(2)}\right|_{1,\Omega_0} \left|e^{(2)}\right|_{1,\Omega} \\ &\lesssim \left|g_0^{(0)} - g_0^{(2)}\right|_{-\frac{1}{2},\gamma_0} \left|e^{(2)}\right|_{1,\Omega} \lesssim |\gamma_0|^{\frac{3}{2(n-1)}} \left|g_0^{(2)}\right|_{1,\gamma_0} \left|e^{(2)}\right|_{1,\Omega}. \end{aligned} \quad (40)$$

Therefore, from (39) and (40),

$$\left|e^{(2)}\right|_{1,\Omega} \lesssim \mathcal{E}_n(u_0^{(0)}) + |\gamma_0|^{\frac{3}{2(n-1)}} \left|g_0^{(2)}\right|_{1,\gamma_0}. \quad (41)$$

Out of all the numerical tests performed (see Section 5.2), we will see that the defeaturing error estimator  $\mathcal{E}_n(u_0^{(0)})$  asymptotically behaves as  $\mathcal{O}\left(|\gamma|^{\frac{n}{2(n-1)}}\right)$  or  $\mathcal{O}\left(|\gamma|^{\frac{n+2}{2(n-1)}}\right)$ , depending on the problem data and geometry. Therefore, since in general  $|\gamma_0| \leq |\gamma|$ , when considering the quadratic Neumann boundary condition  $g_0^{(2)}$  instead of the constant function  $g_0^{(0)}$ , the asymptotic behavior of the error  $|e^{(2)}|_{1,\Omega}$  is the same as the one of  $|e^{(0)}|_{1,\Omega}$ . Indeed, the second term  $|\gamma_0|^{\frac{3}{2(n-1)}} |g_0^{(2)}|_{1,\gamma_0}$  behaves asymptotically at least as  $\mathcal{O}\left(|\gamma|^{\frac{n+2}{2(n-1)}}\right)$  as soon as  $\nabla g_0^{(2)}$  is bounded.

A similar reasoning can be applied to the case of positive features, and we obtain

$$\left|e^{(2)}\right|_{1,\Omega} \lesssim \mathcal{E}_p(\tilde{u}_0^{(0)}) + \left(|\gamma_0|^{\frac{3}{n-1}} \left|g_0^{(2)}\right|_{1,\gamma_0}^2 + |\tilde{\gamma}|^{\frac{3}{n-1}} \left|\tilde{g}^{(2)}\right|_{1,\tilde{\gamma}}^2\right)^{\frac{1}{2}}. \quad (42)$$

The numerical tests performed (see Section 5.2) will show again that, thanks to (42), the asymptotic behavior of  $e^{(0)}$  and  $e^{(2)}$  is the same, and thus the simplest choice of constants  $g_0^{(0)}$  and  $\tilde{g}^{(0)}$  can always be used.

**Remark 4.10** According to the numerical experiments of Section 5, the compatibility conditions (10), (20) and (21) are sufficient but not necessary; the natural extensions of  $f$  in the positive features, and of  $g$  on the boundaries  $\gamma_0$ , also generate optimal estimators.

#### 4.4 Multi-feature a posteriori error estimator

In this section, we will define the defeaturing error estimator in the case of a geometry that presents more than one feature. In doing this, we also consider features that are “close” to one another, or partially superposed. We will then prove the reliability and the efficiency (up to oscillations) of the estimator in this general setting.

Let  $\Omega \subset \mathbb{R}^n$  be an open Lipschitz domain with  $N_p \in \mathbb{N}$  distinct positive Lipschitz geometrical features  $\{F^i\}_{i=1}^{N_p}$ , and  $N_n \in \mathbb{N}$  distinct negative Lipschitz geometrical features  $\{F^j\}_{j=N_p+1}^{N_p+N_n}$ . Let  $N := N_p + N_n$  be the total number of features, and let  $\mathcal{F} := \{F^i\}_{i=1}^{N_p} \cup \{F^j\}_{j=N_p+1}^N$  be the set of all (positive and negative) features. Moreover, let  $\Omega_0$  be the defeatured geometry, that is,

$$\begin{aligned} \Omega &= \text{int} \left( \overline{\Omega_0} \cup \left( \bigcup_{i=1}^{N_p} \overline{F^i} \right) \setminus \left( \bigcup_{j=N_p+1}^N \overline{F^j} \right) \right), \\ F^i \cap \Omega_0 &= \emptyset, \quad \forall i = 1, \dots, N_p, \\ F^j &\subset \Omega_0, \quad \forall j = N_p + 1, \dots, N, \end{aligned}$$

and we also assume that  $\Omega_0$  is an open Lipschitz domain. Furthermore, let  $\mathbf{n}^k \equiv \mathbf{n}_{F^k}$  be the unitary outward normal of  $F^k$ , for all  $k = 1, \dots, N$ , and let  $\mathbf{n}_0$  be the unitary outward normal of  $\Omega_0$ . Let us make the following assumption on the features.

**Assumption 4.11** The features  $\mathcal{F}$  are separated, that is for every  $k, \ell = 1, \dots, N$ ,  $k \neq \ell$ ,

$$F^k \cap F^\ell = \emptyset \quad \text{and} \quad (\partial F^k \cap \partial F^\ell) \subset (\partial \Omega \cup \partial \Omega_0).$$

Moreover, for all  $i = 1, \dots, N_p$ , let  $\tilde{F}^i \subset \mathbb{R}^n$  be a Lipschitz domain such that  $\tilde{F}^i \supset F^i$  and  $(\partial F^i \setminus \overline{\Gamma_N}) \subset \partial \tilde{F}^i$ . Note that we do not require Assumption 4.11 on these extensions of the positive features, that is we could have  $\tilde{F}^k \cap \Omega_0 \neq \emptyset$  or  $\tilde{F}^k \cap \tilde{F}^\ell \neq \emptyset$  for some  $k, \ell = 1, \dots, N$ .

**Remark 4.12** Suppose that  $F^k$  is positive and  $F^\ell$  negative, that is  $k \leq N_p$  and  $\ell > N_p$ . Since  $F^k \subset \Omega$  and  $F^\ell \cap \Omega = \emptyset$  by definition, then  $F^k \cap F^\ell = \emptyset$  and  $(\partial F^k \cap \partial F^\ell) \subset \partial \Omega$ . That is, by definition, they satisfy Assumption 4.11, and can therefore share a part of boundary (see Figure 5). Consequently, if in a given geometry  $\Omega$ , two features  $F^k$  and  $F^\ell$  do not satisfy Assumption 4.11,  $k, \ell = 1, \dots, N$ ,  $k \neq \ell$ , then they are necessarily either both positive or both negative. In this case,  $F^{k,\ell} := \text{int}(\overline{F^k} \cup \overline{F^\ell})$  is a connected set and can be considered as a single (positive or negative) feature that replaces the two features  $F^k$  and  $F^\ell$ . This allows us to always be able to satisfy Assumption 4.11.

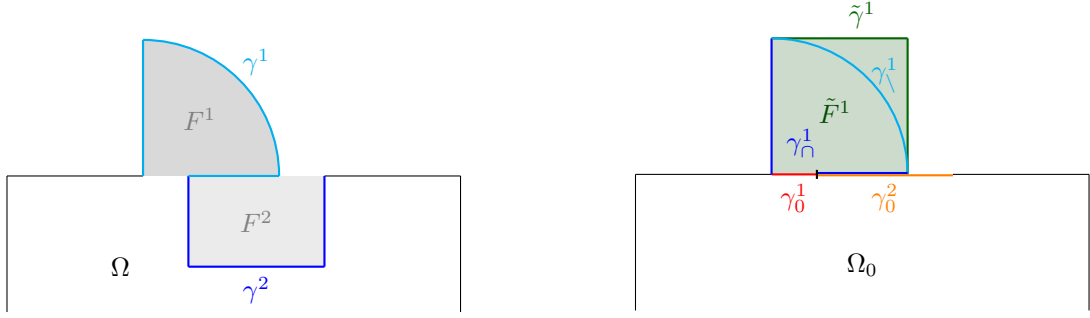
Furthermore, for positive features, let us introduce the notation  $\gamma^i$ ,  $\gamma_\lambda^i$ ,  $\gamma_\cap^i$ ,  $\gamma_0^i$  and  $\tilde{\gamma}^i$  for  $i = 1, \dots, N_p$ , analogous to the single feature case studied in Section 4.2, and for negative features, we introduce the notation  $\gamma^j$  and  $\gamma_0^j$  for  $j = N_p + 1, \dots, N$ , analogous to Section 4.1. More precisely, and as illustrated in Figure 5,

$$\begin{aligned} \forall i = 1, \dots, N_p, & \quad \gamma_0^i := \partial F^i \setminus \overline{\Gamma_N}; \\ \forall j = N_p + 1, \dots, N, & \quad \gamma_0^j := \partial F^j \setminus (\overline{\Gamma_N} \cap \partial(\Omega \cap \Omega_0)), \\ \forall k = 1, \dots, N, & \quad \gamma^k := \partial F^k \setminus \overline{\gamma_0^k}, \\ \forall i = 1, \dots, N_p, & \quad \gamma_\lambda^i := \gamma^i \setminus \partial \tilde{F}^i; \quad \gamma_\cap^i := \text{int}(\gamma^i \cap \partial \tilde{F}^i); \quad \tilde{\gamma}^i := \partial \tilde{F}^i \setminus \partial F^i. \end{aligned}$$

To simplify the notation, let

$$\Gamma := \bigcup_{k=1}^N \gamma^k, \quad \Gamma_p := \bigcup_{i=1}^{N_p} \gamma^i, \quad \Gamma_n := \bigcup_{j=N_p+1}^N \gamma^j, \quad \Gamma_0^\mathcal{F} := \bigcup_{k=1}^N \gamma_0^k, \quad \Gamma_0 := \bigcup_{i=1}^{N_p} \gamma_0^i, \quad \Gamma_\lambda := \bigcup_{i=1}^{N_p} \gamma_\lambda^i,$$





(a) Domain  $\Omega$  with a positive feature  $F^1$  and a negative feature  $F^2$ . (b) Simplified domain  $\Omega_0$ , feature extension  $\tilde{F}^1$ , and different boundaries.

Figure 5: Example of geometry with a negative and a positive feature that share a part of boundary.

and let  $\Sigma := \Sigma_0 \cup \Sigma_\backslash \cup \Sigma_n$ , where

$$\Sigma_0 := \{\gamma_0^i\}_{i=1}^{N_p}, \quad \Sigma_\backslash := \{\gamma_\backslash^i\}_{i=1}^{N_p}, \quad \Sigma_n := \{\gamma_n^j\}_{j=N_p+1}^N.$$

Suppose that for all  $F \in \mathcal{F}$ ,  $\partial F \cap \Gamma_D = \emptyset$ , and that all  $\sigma \in \Sigma$  are isotropic according to Definition 3.1, where the diameter and the convex hull are considered in the manifold  $\partial(\Omega \cap \Omega_0)$  if  $\sigma \in \Sigma_0 \cap \Sigma_n$ , and in the manifold  $\partial F^i$  if  $\sigma = \gamma_\backslash^i \in \Sigma_\backslash$  for some  $i = 1, \dots, N_p$ .

- (i) Let  $u \in H^1(\Omega)$  be the exact solution of problem (2) in the exact domain  $\Omega$ ;
- (ii) let  $u_0 \in H^1(\Omega_0)$  be the solution of a problem analogous to (4) in the simplified domain  $\Omega_0$ , where  $\gamma$  is replaced by  $\Gamma$  and  $\gamma_0$  by  $\gamma_0^F$ ; the choice of the Neumann boundary condition  $g_0 \in H^{\frac{1}{2}}(\Gamma_0^F)$  will be discussed later;
- (iii) for all  $j = N_p + 1, \dots, N$ , let  $u^j := u_0|_{F^j} \in H^1(F^j)$ ;
- (iv) for all  $i = 1, \dots, N_p$ , let  $u^i \in H^1(\tilde{F}^i)$  be the solution of a problem analogous to (7) in the extended positive feature  $\tilde{F}^i$ , that is, the  $\gamma_0^i$ -Dirichlet extension of  $u_0$  in  $\tilde{F}^i$ ; the choice of the Neumann boundary condition on  $\tilde{\gamma}^i$ , called  $g^i \in H^{\frac{1}{2}}(\tilde{\gamma}^i)$ , will be discussed later;
- (v) let  $u_d \in H^1(\Omega)$  be the function such that

$$u_d \equiv \begin{cases} u_0|_{\Omega \cap \Omega_0} & \text{in } \Omega \cap \Omega_0 \\ u^i|_{F^i} & \text{in } F^i, \text{ for all } i = 1, \dots, N_p. \end{cases} \quad (43)$$

With this notation, we define the defeaturing error estimator as

$$\mathcal{E}(u_d) := \left( \sum_{i=1}^{N_p} \mathcal{E}_p^i(u^i)^2 + \sum_{j=N_p+1}^N \mathcal{E}_n^j(u^j)^2 \right)^{\frac{1}{2}}, \quad (44)$$

where  $\mathcal{E}_p^i(u^i)$  is the defeaturing estimator (19) on  $F^i$ , for all the positive features,  $i = 1, \dots, N_p$ ; and  $\mathcal{E}_n^j(u^j)$  is the defeaturing estimator (9) on  $F^j$ , for all the negative features,  $j = N_p + 1, \dots, N$ , i.e.:

$$\begin{aligned} \mathcal{E}_p^i(u^i) &:= \left( \left| \gamma_\backslash^i \right|^{\frac{1}{n-1}} \left\| g - \frac{\partial u^i}{\partial \mathbf{n}^i} \right\|_{0, \gamma_\backslash^i}^2 + \left| \gamma_0^i \right|^{\frac{1}{n-1}} \left\| g_0 + \frac{\partial u^i}{\partial \mathbf{n}^i} \right\|_{0, \gamma_0^i}^2 \right)^{\frac{1}{2}}, \\ \mathcal{E}_n^j(u^j) &:= \left| \gamma^j \right|^{\frac{1}{2(n-1)}} \left\| g + \frac{\partial u^j}{\partial \mathbf{n}^j} \right\|_{0, \gamma^j}. \end{aligned}$$

To simplify the notation, for all  $\sigma \in \Sigma$ , let

$$k_\sigma := \begin{cases} i & \text{if } \sigma \equiv \gamma_0^i \text{ or } \sigma \equiv \gamma_\setminus^i \text{ for some } i = 1, \dots, N_p \\ j & \text{if } \sigma \equiv \gamma^j \text{ for some } j = N_p + 1, \dots, N, \end{cases} \quad (45)$$

and let  $g_\sigma \in H^{\frac{1}{2}}(\sigma)$  such that

$$g_\sigma \equiv \begin{cases} -g & \text{if } \sigma \in \Sigma_n \\ g & \text{if } \sigma \in \Sigma_\setminus \\ -g_0 & \text{if } \sigma \in \Sigma_0. \end{cases} \quad (46)$$

Then the defeaturing error estimator can be rewritten as

$$\mathcal{E}(u_d) := \left( \sum_{\sigma \in \Sigma} |\sigma|^{\frac{1}{n-1}} \left\| g_\sigma - \frac{\partial u^{k_\sigma}}{\partial \mathbf{n}^{k_\sigma}} \right\|_{0,\sigma}^2 \right)^{\frac{1}{2}}.$$

In this section, we show that if the features satisfy Assumption 4.11 and if all  $\sigma \in \Sigma$  are isotropic according to Definition 3.1, then under the compatibility conditions (48), (49) and (50) on the Neumann data  $g_0$  and  $g^i$ ,  $i = 1, \dots, N_p$ , the following holds:

$$|u - u_d|_{1,\Omega} \lesssim \mathcal{E}(u_d), \quad (47)$$

with a hidden constant that is *independent* from the number of features  $N$ . Moreover, assume that all  $\sigma \in \Sigma$  are also regular according to Definition 3.2. Then we also show that

$$\mathcal{E}(u_d) \lesssim |u - u_d|_{1,\Omega} + \text{osc}(u_d),$$

where  $\text{osc}(u_d)$  are oscillations defined in (54).

That is, we show that the quantity  $\mathcal{E}(u_d)$  defined in (44) is an estimator for the defeaturing error that is both reliable (see Theorem 4.13) and efficient up to oscillations (see Theorem 4.14).

#### 4.4.1 Upper bound

In this section, we prove that the error indicator defined in (44) verifies (47). We note that the Neumann data  $g_0$  and  $g^i$ ,  $i = 1, \dots, N_p$ , must satisfy conditions analogous to those explained in Remarks 4.2 and 4.7.

**Theorem 4.13** *Let  $g_0 \in H^{\frac{1}{2}}(\Gamma_0^{\mathcal{F}})$  such that*

$$\int_{\gamma_0^i} g_0 \, ds = \int_{\gamma^i} g \, ds + \int_{F^i} f \, dx, \quad \forall i = 1, \dots, N_p, \quad (48)$$

$$\text{and } \int_{\gamma_0^j} g_0 \, ds = \int_{\gamma^j} g \, ds - \int_{F^j} f \, dx, \quad \forall j = N_p + 1, \dots, N, \quad (49)$$

*and for all  $i = 1, \dots, N_p$ , let  $g^i \in H^{\frac{1}{2}}(\tilde{\gamma}^i)$  such that*

$$\int_{\tilde{\gamma}^i} g^i \, ds = \int_{\gamma_\setminus^i} g \, ds - \int_{\tilde{F}^i \setminus F^i} f \, dx. \quad (50)$$

*If all  $\sigma \in \Sigma$  are isotropic according to Definition 3.1, and if the features  $\mathcal{F}$  satisfy Assumption 4.11, then the defeaturing error in energy norm is bounded in terms of the estimator  $\mathcal{E}(u_d)$  introduced in (44) as follows:*

$$|u - u_d|_{1,\Omega} \lesssim \mathcal{E}(u_d),$$

*where the hidden constant is independent from the number of features  $N$ .*

*Proof.* Let

$$e := u - u_d \in H_{0,\Gamma_D}^1(\Omega).$$

Using arguments similar to Theorems 4.1 and 4.6, we obtain for all  $v_0 \in H_{0,\Gamma_D}^1(\Omega \cap \Omega_0)$ ,

$$\int_{\Omega \cap \Omega_0} \nabla e \cdot \nabla v_0 \, dx = \int_{\Gamma_n} \left( g - \frac{\partial u_0}{\partial \mathbf{n}} \right) v_0 \, ds + \int_{\Gamma_0} \left( \frac{\partial u}{\partial \mathbf{n}_0} - g_0 \right) v_0 \, ds, \quad (51)$$

and for all  $i = 1, \dots, N_p$  and all  $v^i \in H^1(F^i)$ ,

$$\int_{F^i} \nabla e \cdot \nabla v^i \, dx = \int_{\gamma_0^i} \frac{\partial (u - u^i)}{\partial \mathbf{n}^i} v^i \, ds + \int_{\gamma_\lambda^i} \left( g - \frac{\partial u^i}{\partial \mathbf{n}^i} \right) v^i \, ds. \quad (52)$$

Therefore, for all  $v \in H_{0,\Gamma_D}^1(\Omega)$ ,

$$\begin{aligned} \int_{\Omega} \nabla e \cdot \nabla v \, dx &= \int_{\Gamma_n} \left( g + \frac{\partial u_0}{\partial \mathbf{n}^j} \right) v \, ds - \int_{\Gamma_0} \left( g_0 + \frac{\partial u^i}{\partial \mathbf{n}^i} \right) v \, ds + \int_{\Gamma_\lambda} \left( g - \frac{\partial u^i}{\partial \mathbf{n}^i} \right) v \, ds \\ &= - \sum_{\sigma \in \Sigma_n} \int_{\sigma} \left( g_{\sigma} - \frac{\partial u^{k_{\sigma}}}{\partial \mathbf{n}^{k_{\sigma}}} \right) v \, ds + \sum_{\sigma \in \Sigma_0 \cup \Sigma_\lambda} \int_{\sigma} \left( g_{\sigma} - \frac{\partial u^{k_{\sigma}}}{\partial \mathbf{n}^{k_{\sigma}}} \right) v \, ds. \end{aligned} \quad (53)$$

Moreover, thanks to equations (48), (49) and (50),  $g_{\sigma} - \frac{\partial u^{k_{\sigma}}}{\partial \mathbf{n}^{k_{\sigma}}}$  has zero average on  $\sigma$ , for all  $\sigma \in \Sigma$ ; see (14), (29) and (30) for more details. Therefore, if for all  $\sigma \in \Sigma$ , we let

$$\bar{e}^{\sigma} := \frac{1}{|\sigma|} \int_{\sigma} e \, ds,$$

and we take  $v = e \in H_{0,\Gamma_D}^1(\Omega)$  in (53), then by following similar steps as for the proof of Theorem 4.1, using the discrete Cauchy-Schwarz inequality and the trace inequality, we get

$$\begin{aligned} |e|_{1,\Omega}^2 &= - \sum_{\sigma \in \Sigma_n} \int_{\sigma} \left( g_{\sigma} - \frac{\partial u^{k_{\sigma}}}{\partial \mathbf{n}^{k_{\sigma}}} \right) e \, ds + \sum_{\sigma \in \Sigma_0 \cup \Sigma_\lambda} \int_{\sigma} \left( g_{\sigma} - \frac{\partial u^{k_{\sigma}}}{\partial \mathbf{n}^{k_{\sigma}}} \right) e \, ds \\ &= - \sum_{\sigma \in \Sigma_n} \int_{\sigma} \left( g_{\sigma} - \frac{\partial u^{k_{\sigma}}}{\partial \mathbf{n}^{k_{\sigma}}} \right) (e - \bar{e}^{\sigma}) \, ds + \sum_{\sigma \in \Sigma_0 \cup \Sigma_\lambda} \int_{\sigma} \left( g_{\sigma} - \frac{\partial u^{k_{\sigma}}}{\partial \mathbf{n}^{k_{\sigma}}} \right) (e - \bar{e}^{\sigma}) \, ds \\ &\lesssim \sum_{\sigma \in \Sigma} |\sigma|^{\frac{1}{2(n-1)}} \left\| g_{\sigma} - \frac{\partial u^{k_{\sigma}}}{\partial \mathbf{n}^{k_{\sigma}}} \right\|_{0,\sigma} |e|_{\frac{1}{2},\sigma} \leq \left( \sum_{\sigma \in \Sigma} |\sigma|^{\frac{1}{n-1}} \left\| g_{\sigma} - \frac{\partial u^{k_{\sigma}}}{\partial \mathbf{n}^{k_{\sigma}}} \right\|_{0,\sigma}^2 \right)^{\frac{1}{2}} \left( \sum_{\sigma \in \Sigma} |e|_{\frac{1}{2},\sigma}^2 \right)^{\frac{1}{2}} \\ &\leq \mathcal{E}(u_d) \left( \sum_{i=1}^{N_p} |e|_{\frac{1}{2},\partial F^i}^2 + |e|_{\frac{1}{2},\partial(\Omega \cap \Omega_0)}^2 \right)^{\frac{1}{2}} \lesssim \mathcal{E}(u_d) \left( \sum_{i=1}^{N_p} \|e\|_{1,F^i}^2 + \|e\|_{1,\Omega \cap \Omega_0}^2 \right)^{\frac{1}{2}} \lesssim \mathcal{E}(u_d) |e|_{1,\Omega}. \end{aligned}$$

We can conclude by simplifying on both sides.  $\square$

#### 4.4.2 Lower bound

In this section, we prove that the error indicator defined in (44) is efficient, that is it is a lower bound for the defeating error, up to oscillations.

Let  $\mathbf{m} \in \mathbb{N}^n$ , and under the regularity assumption of all  $\sigma \in \Sigma$ , let  $\Pi_{\sigma\mathbf{m}} : H_0^{\frac{1}{2}}(\sigma) \rightarrow \mathbb{Q}_{\mathbf{m},0}^{\text{pw}}(\sigma)$  be the extension of the Clément operator [42] developed in [43] on  $\sigma$ , and let us define  $\Pi_{\mathbf{m}}$  such that  $\Pi_{\mathbf{m}}|_{\sigma} \equiv \Pi_{\sigma\mathbf{m}}$  for all  $\sigma \in \Sigma$ . By abuse of notation, we still write  $\Pi_{\mathbf{m}}$  instead of its restriction to any smooth subdomain  $\sigma_{\ell}$  of  $\sigma$ , for all  $\ell = 1, \dots, L_{\sigma}$  and all  $\sigma \in \Sigma$ .

**Theorem 4.14** Consider the same notation and assumptions as in Theorem 4.13, and assume that all  $\sigma \in \Sigma$  are also regular according to Definition 3.2. Then the defeating error, in energy norm, bounds up to oscillations the estimator  $\mathcal{E}(u_d)$  introduced in (44), that is

$$\mathcal{E}(u_d) \lesssim |u - u_d|_{1,\Omega} + \text{osc}(u_d),$$

with

$$\begin{aligned} \text{osc}(u_d) &:= c_{\text{osc}} \left( \sum_{\sigma \in \Sigma} \sum_{\ell=1}^{L_\sigma} \left\| \left( g_\sigma - \frac{\partial u^{k_\sigma}}{\partial \mathbf{n}^{k_\sigma}} \right) - \Pi_{\mathbf{m}} \left( g_\sigma - \frac{\partial u^{k_\sigma}}{\partial \mathbf{n}^{k_\sigma}} \right) \right\|_{0,\sigma_\ell}^2 \right)^{\frac{1}{2}}, \\ c_{\text{osc}} &:= \max \left( \max_{\tilde{\sigma} \in \widetilde{\Sigma_0 \cup \Sigma_n}} |\tilde{\sigma}|, \max_{i=1,\dots,N_p} \left( |\gamma_0^i \cup \gamma_\setminus^i| \right) \right)^{\frac{1}{2(n-1)}}, \end{aligned} \quad (54)$$

where  $\widetilde{\Sigma_0 \cup \Sigma_n}$  is the set of connected components of  $\Gamma_0 \cup \Gamma_n$ .

**Remark 4.15** The oscillations (54) can also be written as a sum of the oscillations in each of the positive features plus a sum of the oscillations in each negative feature, in the same way as the estimator in (44).

*Proof.* The proof is similar to the ones of Theorems 4.4 and 4.8. Let  $e := u - u_d \in H_{0,\Gamma_D}^1(\Omega)$ . From equation (52), for all  $i = 1, \dots, N_p$  and all  $v^i \in H^1(F^i)$ ,

$$\int_{\gamma_0^i \cup \gamma_\setminus^i} \frac{\partial(u - u^i)}{\partial \mathbf{n}^i} v^i \, ds = \int_{\gamma_0^i} \frac{\partial(u - u^i)}{\partial \mathbf{n}^i} v^i \, ds + \int_{\gamma_\setminus^i} \left( g - \frac{\partial u^i}{\partial \mathbf{n}^i} \right) v^i \, ds = \int_{F^i} \nabla e \cdot \nabla v^i \, dx \leq |e|_{1,F^i} |v^i|_{1,F^i}.$$

And from equation (51), if we let  $\mathbf{n}_\delta \equiv \mathbf{n}$  on  $\Gamma_n$  and  $\mathbf{n}_\delta \equiv \mathbf{n}_0$  on  $\Gamma_0$ , then for all  $v_0 \in H_{0,\Gamma_D}^1(\Omega \cap \Omega_0)$ ,

$$\begin{aligned} \int_{\Gamma_n \cup \Gamma_0} \frac{\partial(u - u_0)}{\partial \mathbf{n}_\delta} v_0 \, ds &= \int_{\Gamma_n} \left( g - \frac{\partial u_0}{\partial \mathbf{n}} \right) v_0 \, ds + \int_{\Gamma_0} \left( \frac{\partial u}{\partial \mathbf{n}_0} - g_0 \right) v_0 \, ds \\ &= \int_{\Omega \cap \Omega_0} \nabla e \cdot \nabla v_0 \, dx \leq |e|_{1,\Omega \cap \Omega_0} |v_0|_{1,\Omega \cap \Omega_0}. \end{aligned}$$

Therefore, by the same argument as in Theorems 4.8 and 4.4, for all  $i = 1, \dots, N_p$ ,

$$\left\| \frac{\partial(u - u^i)}{\partial \mathbf{n}^i} \right\|_{H_{00}^{-1/2}(\gamma_0^i \cup \gamma_\setminus^i)} \lesssim |e|_{1,F^i}; \quad \left\| \frac{\partial(u - u_0)}{\partial \mathbf{n}_\delta} \right\|_{H_{00}^{-1/2}(\Gamma_n \cup \Gamma_0)} \lesssim |e|_{1,\Omega \cap \Omega_0}. \quad (55)$$

Thus from (55),

$$\left( \sum_{i=1}^{N_p} \left\| \frac{\partial(u - u^i)}{\partial \mathbf{n}^i} \right\|_{H_{00}^{-1/2}(\gamma_0^i \cup \gamma_\setminus^i)}^2 + \left\| \frac{\partial(u - u_0)}{\partial \mathbf{n}_\delta} \right\|_{H_{00}^{-1/2}(\Gamma_n \cup \Gamma_0)}^2 \right)^{\frac{1}{2}} \lesssim \left( \sum_{i=1}^{N_p} |e|_{1,F^i}^2 + |e|_{1,\Omega \cap \Omega_0}^2 \right)^{\frac{1}{2}} = |e|_{1,\Omega}. \quad (56)$$

Moreover, note that

$$\begin{aligned} \text{on all } \sigma \in \Sigma_0, \quad g_\sigma &= -g_0 = -\frac{\partial u^{k_\sigma}}{\partial \mathbf{n}_\delta} \neq \frac{\partial u^{k_\sigma}}{\partial \mathbf{n}^{k_\sigma}} \text{ and } \frac{\partial u}{\partial \mathbf{n}_\delta} = -\frac{\partial u}{\partial \mathbf{n}^{k_\sigma}}, \\ \text{on all } \sigma \in \Sigma_\setminus, \quad g_\sigma &= g = \frac{\partial u}{\partial \mathbf{n}} = \frac{\partial u}{\partial \mathbf{n}^{k_\sigma}}, \\ \text{on all } \sigma \in \Sigma_n, \quad g_\sigma &= -g = -\frac{\partial u}{\partial \mathbf{n}_\delta} \text{ and } \frac{\partial u^{k_\sigma}}{\partial \mathbf{n}^{k_\sigma}} = -\frac{\partial u^{k_\sigma}}{\partial \mathbf{n}_\delta}. \end{aligned}$$

Therefore, from this observation, from (56), and by inverse inequality of Lemma A.3,

$$\begin{aligned}
\mathcal{E}(u_d)^2 &\lesssim \sum_{\sigma \in \Sigma_0 \cup \Sigma_n} |\sigma|^{\frac{1}{n-1}} \left\| \frac{\partial(u - u^{k_\sigma})}{\partial \mathbf{n}_\delta} \right\|_{0,\sigma}^2 + \sum_{\sigma \in \Sigma_0 \cup \Sigma_n} |\sigma|^{\frac{1}{n-1}} \left\| \frac{\partial(u - u^{k_\sigma})}{\partial \mathbf{n}^{k_\sigma}} \right\|_{0,\sigma}^2 \\
&\lesssim \left\| \frac{\partial(u - u_d)}{\partial \mathbf{n}_\delta} \right\|_{H_{00}^{-1/2}(\Gamma_0 \cup \Gamma_n)}^2 + \left\| \left( \frac{\partial(u - u_d)}{\partial \mathbf{n}_\delta} \right) - \Pi_{\mathbf{m}} \left( \frac{\partial(u - u_d)}{\partial \mathbf{n}_\delta} \right) \right\|_{H_{00}^{-1/2}(\Gamma_0 \cup \Gamma_n)}^2 \\
&\quad + \sum_{i=1}^{N_p} \left( \left\| \frac{\partial(u - u^i)}{\partial \mathbf{n}^i} \right\|_{H_{00}^{-1/2}(\gamma_0^i \cup \gamma_\chi^i)}^2 + \left\| \frac{\partial(u - u^i)}{\partial \mathbf{n}^i} - \Pi_{\mathbf{m}} \left( \frac{\partial(u - u^i)}{\partial \mathbf{n}^i} \right) \right\|_{H_{00}^{-1/2}(\gamma_0^i \cup \gamma_\chi^i)}^2 \right) \\
&\quad + \text{osc}(u_d)^2 \\
&\lesssim |e|_{1,\Omega}^2 + \max_{\tilde{\sigma} \in \Sigma_0 \cup \Sigma_n} (|\tilde{\sigma}|)^{\frac{1}{n-1}} \left\| \left( \frac{\partial(u - u_d)}{\partial \mathbf{n}_\delta} \right) - \Pi_{\mathbf{m}} \left( \frac{\partial(u - u_d)}{\partial \mathbf{n}_\delta} \right) \right\|_{0,\Gamma_0 \cup \Gamma_n}^2 \\
&\quad + \sum_{i=1}^{N_p} |\gamma_0^i \cup \gamma_\chi^i|^{\frac{1}{n-1}} \left\| \frac{\partial(u - u^i)}{\partial \mathbf{n}^i} - \Pi_{\mathbf{m}} \left( \frac{\partial(u - u^i)}{\partial \mathbf{n}^i} \right) \right\|_{0,\gamma_0^i \cup \gamma_\chi^i}^2 \\
&\lesssim \left( |e|_{1,\Omega} + \text{osc}(u_d) \right)^2,
\end{aligned} \tag{57}$$

where inequality (57) has been obtained thanks to Lemma A.4.  $\square$

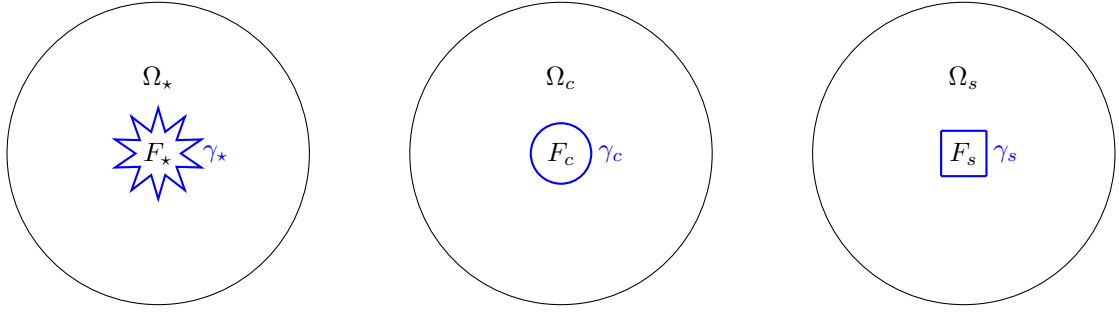
## 5 Numerical considerations and experiments

From the definition of the a posteriori defeaturing error estimator (44), to estimate the error introduced by defeaturing the problem geometry, we only need to perform the following steps.

1. Choose the Neumann data  $g_0$  that satisfies the flux conservation assumptions (48) and (49), and solve the defeatured problem (3).
2. For each positive feature  $F^i$ ,  $i = 1, \dots, N_p$ , choose the Neumann data  $g^i$  that satisfies the flux conservation assumptions (50), and solve the local extension problem (5). However, features may be geometrically complex, and the solution of the extension problem an unwanted burden. Therefore, instead of (5), one can solve the extension problem (6) in a chosen (simple) domain  $\tilde{F}^i$  that contains  $F^i$  and such that  $\gamma_0^i \subset \partial \tilde{F}^i$ .
3. Compute the boundary integrals  $\left\| g_\sigma - \frac{\partial u^{k_\sigma}}{\partial \mathbf{n}^{k_\sigma}} \right\|_{0,\sigma}$  for each  $\sigma \in \Sigma$ , as defined in (45), (46). That is, we suitably evaluate the error made on the normal derivative of the solution on specific parts of the boundaries of the features.

The way to choose  $g_0$  and  $g^i$ ,  $i = 1, \dots, N_p$ , has been discussed in Section 4.3.

In the remaining part of the paper, we consider numerical examples to illustrate the validity of our defeaturing error estimator. All the numerical experiments presented in the following section have been implemented in GeoPDEs [44], an open-source and free Octave/Matlab package for the resolution of partial differential equations specifically designed for isogeometric analysis [2]. Moreover, a very fine mesh is used in order to be able to neglect the error due to the numerical approximation.



(a) Domain with a star feature. (b) Domain with a circle feature. (c) Domain with a square feature.

Figure 6: Comparison between feature shapes.

$\Omega$	Perimeter( $F$ )	Area( $F$ )	$\mathcal{E}(u_0)$	$ u - u_0 _{1,\Omega}$	Eff. index
$\Omega_\star, r_\star = 1.83 \cdot 10^{-2}$	0.400	$2.07 \cdot 10^{-3}$	$4.68 \cdot 10^{-2}$	$1.10 \cdot 10^{-2}$	4.24
$\Omega_c, r_c = 6.37 \cdot 10^{-2}$	0.400	$1.27 \cdot 10^{-2}$	$4.70 \cdot 10^{-2}$	$1.86 \cdot 10^{-2}$	2.52
$\Omega_s, r_s = 5.00 \cdot 10^{-2}$	0.400	$1.00 \cdot 10^{-2}$	$4.70 \cdot 10^{-2}$	$1.80 \cdot 10^{-2}$	2.61
$\Omega_c, r_c = 5.64 \cdot 10^{-2}$	0.355	$1.00 \cdot 10^{-2}$	$4.16 \cdot 10^{-2}$	$1.65 \cdot 10^{-2}$	2.52
$\Omega_\star, r_\star = 4.02 \cdot 10^{-2}$	0.880	$1.00 \cdot 10^{-2}$	$1.03 \cdot 10^{-1}$	$2.44 \cdot 10^{-2}$	4.23

Table 1: Results of the comparison between feature shapes.

## 5.1 Impact of some properties on the defeaturing error

While validating the theory developed in Section 4.1, we study the impact of the shape and the size of a feature on the defeaturing error and estimator, and of the choice of the defeatured Neumann data. Moreover, we show that our estimator is able to tell when a small feature largely impacts the defeaturing error, and inversely, it can tell when a large feature does not impact much the error.

### 5.1.1 Feature shape

In this example, we compare the behavior of the error and the estimator on the same Poisson problem in three different geometries: one with a star-shaped feature, another one with a circular feature, and the last one with a squared feature. Let

$$\Omega_0 := \{(r \cos(\theta), r \sin(\theta)) \in \mathbb{R}^2 : 0 \leq r < 1, 0 \leq \theta \leq 2\pi\},$$

let  $\Omega_\star := \Omega_0 \setminus \overline{F_\star}$ ,  $\Omega_c := \Omega_0 \setminus \overline{F_c}$  and  $\Omega_s := \Omega_0 \setminus \overline{F_s}$ , with

- $F_\star$  the 10-branch regular star of inner radius  $r_\star > 0$ , outer radius  $2r_\star$ , centered in  $(0, 0)$ ,
- $F_c$  the circle of radius  $r_c > 0$ , centered in  $(0, 0)$ ,
- $F_s$  the square of size  $2r_s > 0$ , centered in  $(0, 0)$ ,

as in Figure 6.

We choose  $r_\star, r_c, r_s > 0$  such that  $F_\star, F_c$  and  $F_s$  have, first, the same area, and then, the same perimeter. We consider Poisson problem (1) solved in  $\Omega_\star, \Omega_c$  and in  $\Omega_s$ , and its defeatured version (3). We take in  $\Omega_0$   $f(r, \theta) = 1$  if  $r > 0.1$  and  $f(r, \theta) = 0$  otherwise,  $h \equiv 0$  on  $\Gamma_D := \partial\Omega_0$  and  $g \equiv 0$  on  $\gamma_\star := \partial F_\star$ ,  $\gamma_c := \partial F_c$  and on  $\gamma_s := \partial F_s$ . We remark that the compatibility condition (10) on the Neumann data is satisfied.

The results are summarized in Table 1. We can see that in all the cases, the larger the perimeter or the area of the feature, the larger the defeaturing error and estimator. Moreover, the effectivity index remains equal when considering the same feature but with different dimensions: this shows that it is indeed independent

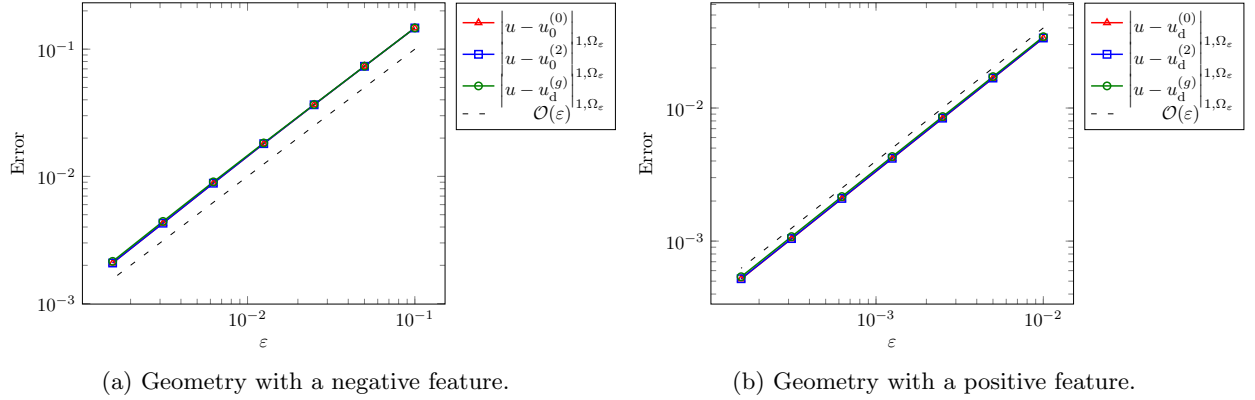


Figure 7: Comparison between solutions obtained with different defeatured Neumann boundary conditions, in two different geometries.

from the measure of the considered feature and its boundary. Moreover, the shape of the feature does not impact much the defeaturing estimator: we do not observe any major difference between the smooth feature (the circle), the convex non-smooth Lipschitz feature (the square), and the non-convex non-smooth Lipschitz feature (the star). Our theory indeed treats those different types of geometries in a unique way.

### 5.1.2 Comparison of defeatured Neumann data

In Section 4.3, the way to choose the Neumann data  $g_0$  and  $\tilde{g}$  (or  $g^i$ ,  $i = 1, \dots, N_p$  in the multi-feature case) is discussed. Numerical examples are presented in this section to illustrate the fact that it is enough to choose  $g_0$  and  $\tilde{g}$  as the natural extension of the Neumann data  $g$  in order to obtain the optimal convergence rate of the defeaturing error with respect to the size of the features, even if this choice does not satisfy the compatibility conditions (10), (20) and (21).

Let us first consider a geometry with one negative feature. Let  $\varepsilon = \frac{10^{-2}}{2^k}$  for  $k = 0, 1, \dots, 6$ , and  $\Omega_\varepsilon := \Omega_0 \setminus \overline{F_\varepsilon}$  with  $\Omega_0 := (0, 1)^2$  and

$$F_\varepsilon := \left\{ (x, y) \in \mathbb{R}^2 : 0.5 - \frac{\varepsilon}{2} < x < 0.5 + \frac{\varepsilon}{2}, 1 - \varepsilon < y < 1 \right\},$$

as in Figure 2a. We consider Poisson problem (1) solved in  $\Omega_\varepsilon$ , and its defeatured version (3) in  $\Omega_0$ . We take  $f \equiv 0$  in  $\Omega_0$ ,  $h(x, y) = 40 \cos(\pi x) + 10 \cos(5\pi x)$  on

$$\Gamma_D := \{(x, 0) \in \mathbb{R}^2 : 0 < x < 1\},$$

and  $g(x, y) = x^2 + (1 - y)^3$  on  $\Gamma_N := \partial\Omega_\varepsilon \setminus \overline{\Gamma_D}$ . We first solve (3) with the constant function  $g_0 := g_0^{(0)}$ , then solve it with the quadratic function  $g_0 := g_0^{(2)}$ , as defined at the beginning of Section 4.3. Finally, we solve it with the natural extension of  $g$  in  $\gamma_0$ , that is  $g_0 := g$ . We respectively obtain  $u_0^{(0)}$ ,  $u_0^{(2)}$  and  $u_0^{(g)}$ . In Figure 7a,

the errors  $|u - u_0^{(0)}|_{1,\Omega}$ ,  $|u - u_0^{(2)}|_{1,\Omega}$  and  $|u - u_0^{(g)}|_{1,\Omega}$  are almost indistinguishable but  $\frac{|u - u_0^{(2)}|_{1,\Omega}}{|u - u_0^{(0)}|_{1,\Omega}}$  varies

between 1.0001 and 1.0002, and  $\frac{|u - u_0^{(g)}|_{1,\Omega}}{|u - u_0^{(0)}|_{1,\Omega}}$  varies between 1.001 and 1.030. We can see that the three errors have the same asymptotic behavior with respect to  $\varepsilon$ , that is with respect to the measure of  $\gamma$ .

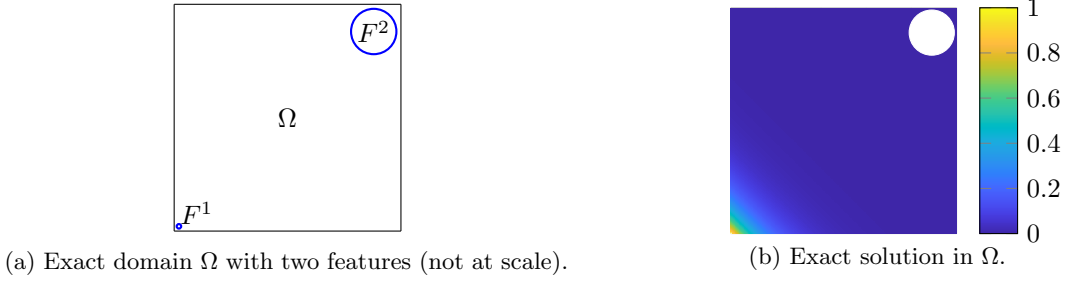


Figure 8: Geometry with two features of different size and exact solution.

$\mathcal{E}_n^1(u_0)$	$\mathcal{E}_n^2(u_0)$	$\mathcal{E}(u_0)$	$ u - u_0 _{1,\Omega}$	Effectivity index
$4.93 \cdot 10^{-2}$	$6.32 \cdot 10^{-6}$	$4.93 \cdot 10^{-2}$	$1.44 \cdot 10^{-2}$	3.43

Table 2: Results of the comparison between feature sizes.

Let us now consider a geometry with one positive feature. Let  $\Omega_0$ ,  $\Gamma_D$ ,  $f$ ,  $h$  and  $g$  be as before, and let  $\Omega_\varepsilon := \text{int}(\overline{\Omega_0} \cup \overline{F_\varepsilon})$  with

$$F_\varepsilon := \left\{ (x, y) \in \mathbb{R}^2 : 0.5 - \frac{\varepsilon}{2} < x < 0.5 + \frac{\varepsilon}{2}, 1 < y < 1 + \varepsilon \right\},$$

as in Figure 2c. Let  $\Gamma_N := \partial\Omega_\varepsilon \setminus \overline{\Gamma_D}$ . We consider the same Poisson problem (1) as before, but solved in this  $\Omega_\varepsilon$ . We also solve its defeatured version (3) in  $\Omega_0$ , first with  $g_0 := g_0^{(0)}$ , then with  $g_0 := g_0^{(2)}$ , and finally with the natural extension of  $g$  in  $\gamma_0$ ,  $g_0 := g$ . Then we extend both defeatured solutions to  $F_\varepsilon$  by (6) with  $\tilde{F} := F_\varepsilon$ . We respectively obtain  $u_d^{(0)}$ ,  $u_d^{(2)}$  and  $u_d^{(g)}$ . In Figure 7b, the errors  $|u - u_d^{(0)}|_{1,\Omega}$ ,  $|u - u_d^{(2)}|_{1,\Omega}$  and

$|u - u_d^{(g)}|_{1,\Omega}$  are almost indistinguishable but  $\frac{|u - u_d^{(2)}|_{1,\Omega}}{|u - u_d^{(0)}|_{1,\Omega}}$  varies between 1.002 and 1.004, and  $\frac{|u - u_d^{(g)}|_{1,\Omega}}{|u - u_d^{(0)}|_{1,\Omega}}$

varies between 1.025 and 1.039. We can see that as for the positive feature case, the three errors have the same asymptotic behavior with respect to  $\varepsilon$ , that is with respect to the measure of  $\gamma_0$ .

Therefore, one can always choose  $g_0$  and  $\tilde{g}$  as the natural extension of  $g$  on  $\gamma_0$  and  $\tilde{\gamma}$ , respectively, as this is the simplest choice one can make.

**Remark 5.1** Analogously, one can choose to consider the natural extension of  $f$  in the positive features, even if it does not verify the compatibility conditions (10), (20) and (21), while still obtaining the optimal convergence rate of the defeaturing error with respect to the size of the features. In particular, this is the choice one would like to make when considering internal features, that is features for which  $\gamma_0 = \emptyset$ .

### 5.1.3 Feature size

Removing a small feature where the solution of the PDE has a high gradient can increase notably the defeaturing error, while the error might almost not be affected when removing a large feature where the solution of the PDE is nearly constant. The following example shows that our estimator is also able to capture this. Let  $\Omega_0 := (0, 1)^2$  and  $\Omega := \Omega_0 \setminus (\overline{F^1} \cup \overline{F^2})$ , where  $F^1$  and  $F^2$  are circles of two different sizes given by

$$\begin{aligned} F^1 &:= \{(1.1 \cdot 10^{-3}, 1.1 \cdot 10^{-3}) + (r \cos(\theta), r \sin(\theta)) \in \mathbb{R}^2 : 0 \leq r < 10^{-3}, 0 \leq \theta \leq 2\pi\}, \\ F^2 &:= \{(8.9 \cdot 10^{-1}, 8.9 \cdot 10^{-1}) + (r \cos(\theta), r \sin(\theta)) \in \mathbb{R}^2 : 0 \leq r < 10^{-1}, 0 \leq \theta \leq 2\pi\}, \end{aligned}$$



similarly as in Figure 8a. We consider Poisson problem (1) solved in  $\Omega$ , and its defeatured version (3) in  $\Omega_0$ . We take  $f(x, y) := -128e^{-8(x+y)}$  in  $\Omega_0$ ,  $h(x, y) := e^{-8(x+y)}$  on

$$\Gamma_D := \{(x, 0), (0, y) \in \mathbb{R}^2 : 0 \leq x, y < 1\},$$

the bottom and left sides,  $g(x, y) := -8e^{-8(x+y)}$  on  $\partial\Omega_0 \setminus \overline{\Gamma_D}$  and  $g \equiv 0$  on  $\partial F_1 \cup \partial F_2$ .

With this choice, the solution to Poisson problem has a very high gradient near feature  $F^1$ , and it is almost constantly zero near feature  $F^2$ , as we can observe in Figure 8b. Therefore, one can expect the presence of  $F^1$  to be more important than  $F^2$  with respect to the solution accuracy, even if  $F^1$  is notably smaller than  $F^2$ . The results are presented in Table 2, where we can see that this is indeed the case: the estimator on  $F^2$  is four orders of magnitude smaller than the estimator on  $F^1$ , even if the radius of  $F^1$  is two orders of magnitude smaller than the one of  $F^2$ . This confirms the fact our estimator as written in (44) correctly trades off the measure of the features and their position in the differential domain, in order to correctly assess the impact of defeaturing on the solution.

## 5.2 Error convergence with respect to the feature size

We then analyze, in the case of a geometry with a single feature, the convergence of our estimator with respect to the size of the feature. We compare it with the convergence of the defeaturing error.

### 5.2.1 2D geometries

We begin with 2D examples of geometries with one negative feature. Let  $\varepsilon = \frac{10^{-2}}{2^k}$  for  $k = 0, 1, \dots, 6$ , and  $\Omega_\varepsilon^i := \Omega_0 \setminus \overline{F_\varepsilon^i}$  for  $i = 1, 2$  with  $\Omega_0 := (0, 1)^2$  and

$$F_\varepsilon^1 := \{(0.5 + r \cos(\theta), 1 + r \sin(\theta)) \in \mathbb{R}^2 : 0 \leq r < \varepsilon, -\pi < \theta < 0\}, \quad F_\varepsilon^2 := (1 - \varepsilon, 1)^2,$$

as in Figures 9a and 9b. For  $i = 1, 2$ , we consider Poisson problem (1) solved in  $\Omega_\varepsilon^i$ , and its defeatured version (3) in  $\Omega_0$ . We take  $f(x, y) := 10 \cos(3\pi x) \sin(5\pi y)$  in  $\Omega_0$ ,  $h \equiv 0$  on

$$\Gamma_D := \{(x, 0) \in \mathbb{R}^2 : 0 < x < 1\},$$

and  $g \equiv 0$  on  $\Gamma_N := \partial\Omega_\varepsilon^i \setminus \overline{\Gamma_D}$ . In order to satisfy (10), we take  $g_0 \equiv -\frac{1}{|\gamma_0|} \int_{F_\varepsilon^i} f \, dx$  on  $\partial\Omega_0 \setminus \partial\Omega_\varepsilon^i$ .

The results are presented in Figure 10a. Both the error and the estimator converge with respect to the size of the feature as  $\varepsilon \propto |\gamma|$  in the first geometry  $\Omega_\varepsilon^1$ , and as  $\varepsilon^2 \propto |\gamma|^2$  in the second geometry  $\Omega_\varepsilon^2$ . Moreover, the effectivity index is indeed independent from the size of the feature since it remains nearly equal to 1.78 and 1.71, respectively, and for all values of  $\varepsilon$ . That is, as predicted by the theory since the estimator is both reliable (Theorem 4.1) and efficient up to oscillations (Theorem 4.4), in dimension 2, the dependence of the estimator with respect to the size of the feature is explicit.

Let us now consider 2D examples of geometries with one positive feature. Let  $\Omega_0$ ,  $\Gamma_D$ ,  $f$ ,  $h$  and  $g$  be as before, and let  $\Omega_\varepsilon^j := \text{int}(\overline{\Omega_0} \cup \overline{F_\varepsilon^j})$  for  $j = 3, 4$  with

$$F_\varepsilon^3 := \{(0.5 + r \cos(\theta), 1 + r \sin(\theta)) \in \mathbb{R}^2 : 0 \leq r < \varepsilon, 0 < \theta < \pi\}, \quad F_\varepsilon^4 := (1 - \varepsilon, 1) \times (1, 1 + \varepsilon),$$

as in Figures 9c and 9d. Let  $\Gamma_N := \partial\Omega_\varepsilon^j \setminus \overline{\Gamma_D}$ . For each  $j = 3, 4$ , we consider the same Poisson problem (1) as before, but solved in  $\Omega_\varepsilon^j$ . We also solve its defeatured version (3) in  $\Omega_0$  with  $g_0 \equiv \frac{1}{|\gamma_0|} \int_{F_\varepsilon^j} f \, dx$  on  $\partial\Omega_0 \setminus \partial\Omega_\varepsilon^j$  in order to satisfy (20). Then we extend the defeatured solution to  $F_\varepsilon^j$  by (6) with  $\tilde{F} := F_\varepsilon^j$ .

The results are presented in Figure 10b. As for the negative feature case, the error in  $\Omega_0$ , the error in  $F_\varepsilon$  and the estimator converge with respect to the size of the feature as  $\varepsilon \propto |\gamma_0|$  in the first geometry  $\Omega_\varepsilon^3$ , and

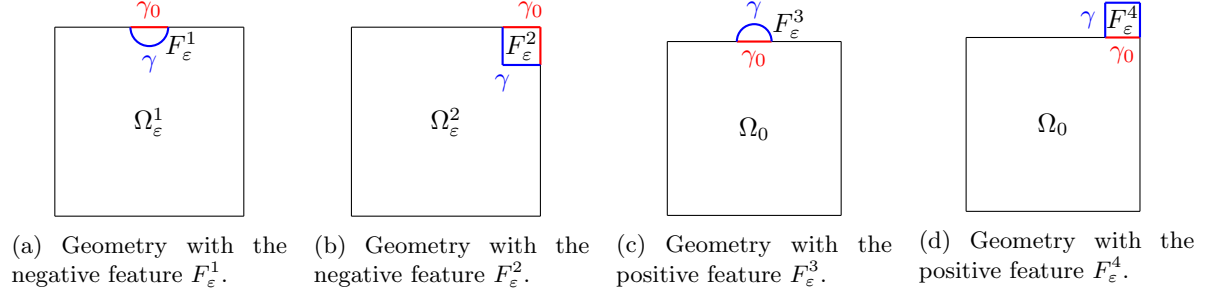


Figure 9: 2D geometries  $\Omega_\varepsilon^k$ ,  $k = 1, 2, 3, 4$ .

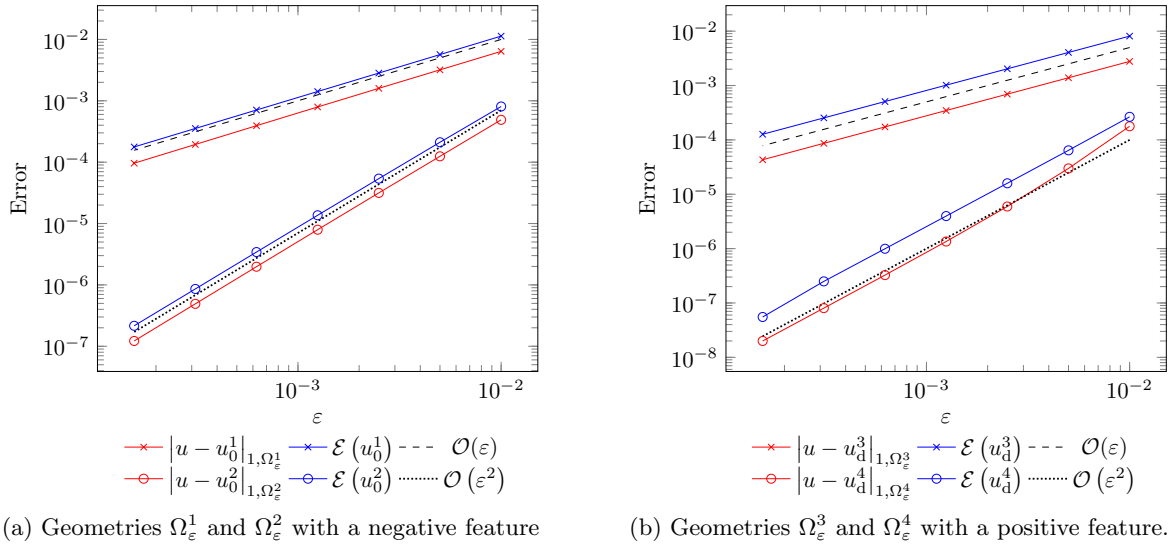


Figure 10: Convergence of the error in 2D domains with one feature.

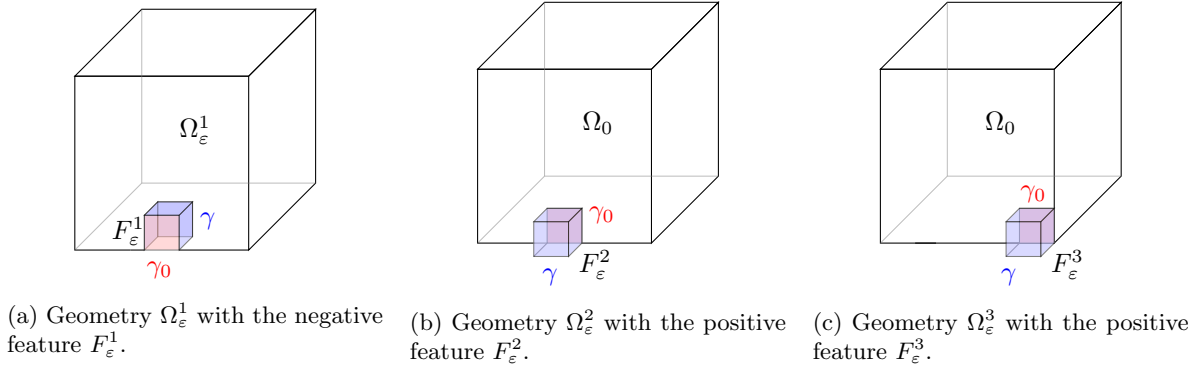


Figure 11: 3D geometries  $\Omega_\varepsilon^k$ ,  $k = 1, \dots, 3$ .

as  $\varepsilon^2 \propto |\gamma|^2$  in the second geometry  $\Omega_\varepsilon^4$ . Moreover, the effectivity index is indeed almost independent from the size of the feature since it remains nearly equal to 2.93 and 2.78, respectively, for all values of  $\varepsilon$ . That is, as predicted by the theory since the estimator is both reliable (Theorem 4.6) and efficient up to oscillations (Theorem 4.8), in dimension 2, the dependence of the estimator with respect to the size of the feature is explicit.

Intuitively, the two observed convergence rates of the defeaturing error and estimator are the ones expected. Indeed, in the geometries  $\Omega_\varepsilon^2$  and  $\Omega_\varepsilon^4$ , the error in the normal derivative  $\frac{\partial u_0}{\partial \mathbf{n}_F}$  on  $\gamma$  and  $\gamma_0$ , respectively, is of size at most  $\varepsilon$  since  $\frac{\partial u_0}{\partial \mathbf{n}} = \frac{\partial u}{\partial \mathbf{n}}$  on  $\partial\Omega \setminus \gamma$  and  $\partial F \setminus \gamma_0$ , respectively. Therefore,  $\left\| g + \frac{\partial u_0^2}{\partial \mathbf{n}_F} \right\|_{0,\gamma} \approx \varepsilon^{\frac{3}{2}} = |\gamma|^{\frac{3}{2}}$  and  $\left\| g_0 + \frac{\partial u_0^4}{\partial \mathbf{n}_F} \right\|_{0,\gamma_0} \approx \varepsilon^{\frac{3}{2}} = |\gamma|^{\frac{3}{2}}$ , and thus in both cases, the estimator has a convergence rate of  $\varepsilon^2$ . Instead, in the geometries  $\Omega_\varepsilon^1$  and  $\Omega_\varepsilon^3$ , the error in the normal derivative  $\frac{\partial u_0}{\partial \mathbf{n}_F}$  on  $\gamma$  and  $\gamma_0$ , respectively, is of size 1, since the imposed boundary conditions guarantee it to be of size at most  $\varepsilon$  in only one direction in space, due to the geometry of the problem. Therefore,  $\left\| g + \frac{\partial u_0^1}{\partial \mathbf{n}_F} \right\|_{0,\gamma} \approx \varepsilon^{\frac{1}{2}} = |\gamma|^{\frac{1}{2}}$  and  $\left\| g_0 + \frac{\partial u_0^3}{\partial \mathbf{n}_F} \right\|_{0,\gamma_0} \approx \varepsilon^{\frac{1}{2}} = |\gamma|^{\frac{1}{2}}$ , and thus in both cases, the estimator has a convergence rate of  $\varepsilon$ . This will also be observed in 3 dimensions in the next section.

### 5.2.2 3D geometries

Let us first consider a 3D example of a geometry with one negative feature. Let  $\varepsilon = \frac{10^{-2}}{2^k}$  for  $k = 0, 1, \dots, 6$ , and  $\Omega_\varepsilon := \Omega_0 \setminus \overline{F_\varepsilon}$  with  $\Omega_0 := (0, 1)^3$  and

$$F_\varepsilon := \left\{ (x, y, z) \in \mathbb{R}^3 : 0.5 - \frac{\varepsilon}{2} < x < 0.5 + \frac{\varepsilon}{2}, 1 - \varepsilon < y < 1, 0 < z < \varepsilon \right\},$$

as in Figure 11a. We consider Poisson problem (1) solved in  $\Omega_\varepsilon$ , and its defeatured version (3) on  $\Omega_0$ . We take  $f(x, y) := 10 \cos(3\pi x) \sin(5\pi y) \sin(7\pi z)$  in  $\Omega$ ,  $h \equiv 0$  on

$$\Gamma_D := \{(x, 0, z) \in \mathbb{R}^3 : 0 < x, z < 1\},$$

and  $g \equiv 0$  on  $\Gamma_N := \partial\Omega_\varepsilon \setminus \overline{\Gamma_D}$ . In order to satisfy (10), we take  $g_0 \equiv -\frac{1}{|\gamma_0|} \int_{F_\varepsilon} f \, dx$  on  $\partial\Omega_0 \setminus \partial\Omega_\varepsilon$ .

The results are presented in Figure 12a. The error in  $\Omega_0$ , the error in  $F_\varepsilon$  and the estimator converge with respect to the size of the feature as  $\varepsilon^{\frac{3}{2}} \propto |\gamma_0|^{\frac{3}{4}}$ , and the effectivity index is indeed independent from the size

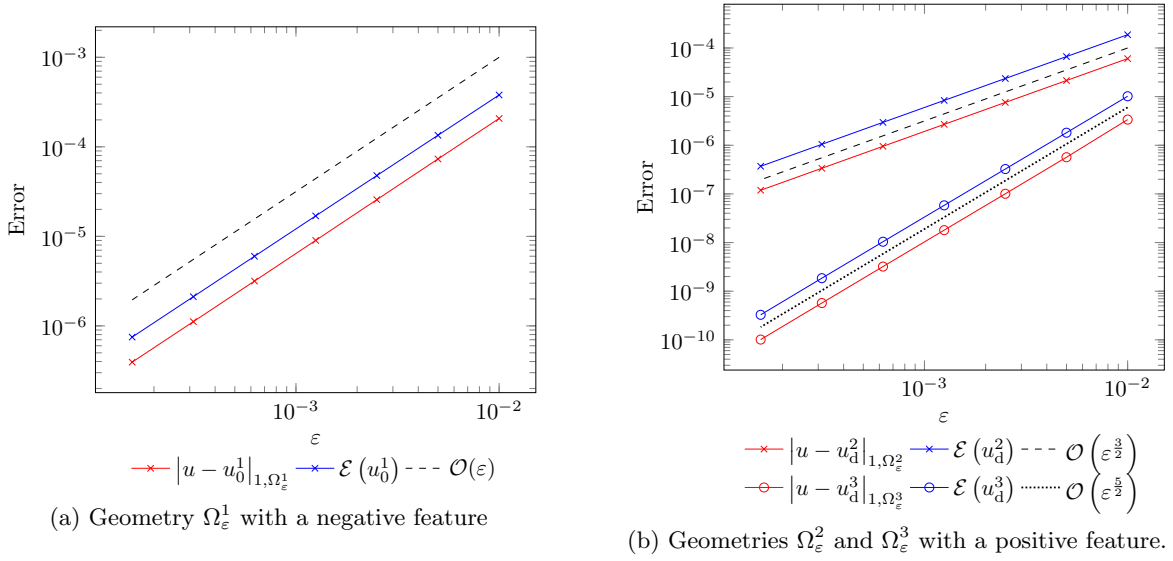


Figure 12: Convergence of the error in 3D domains with one feature.

of the feature since it remains equal to 1.87 for all values of  $\varepsilon$ . That is, again as predicted by the theory since the estimator is both reliable (Theorem 4.1) and efficient up to oscillations (Theorem 4.4), in dimension 3, the dependence of the estimator with respect to the size of the feature is explicit. Intuitively, the observed convergence rate of the defeaturing error and estimator is the one expected, as it has been discussed in the 2D examples of Section 5.2.1.

Let us now consider 3D examples of geometries with one positive feature. Let  $\Omega_0$ ,  $\Gamma_D$ ,  $f$ ,  $h$ , and  $g$  be as before, and let  $\Omega_\varepsilon^j := \text{int}(\overline{\Omega_0} \cup F_\varepsilon^j)$  for  $j = 2, 3$  with

$$F_\varepsilon^2 := \left\{ (x, y, z) \in \mathbb{R}^3 : 0.5 - \frac{\varepsilon}{2} < x < 0.5 + \frac{\varepsilon}{2}, 1 < y < 1 + \varepsilon, 0 < z < \varepsilon \right\}, \quad F_\varepsilon^3 := F_\varepsilon^2 + \left( 0.5 - \frac{\varepsilon}{2}, 0, 0 \right),$$

as in Figures 11b and 11c. Let  $\Gamma_N := \partial\Omega_\varepsilon^j \setminus \overline{\Gamma_D}$ . For each  $j = 2, 3$ , we consider the same Poisson problem (1) as before, but solved in this  $\Omega_\varepsilon^j$ . We also solve its defeatured version (3) in  $\Omega_0$  with  $g_0 \equiv \frac{1}{|\gamma_0|} \int_{F_\varepsilon^j} f \, dx$  on  $\partial\Omega_0 \setminus \partial\Omega_\varepsilon$  in order to satisfy (20). Then we extend the defeatured solution to  $F_\varepsilon^j$  by (6) with  $\tilde{F} := F_\varepsilon^j$ .

The results are presented in Figure 12b. As for the negative feature case, the error in  $\Omega_0$ , the error in  $F_\varepsilon$  and the estimator converge with respect to the size of the feature as  $\varepsilon^{\frac{3}{2}} \propto |\gamma_0|^{\frac{3}{4}}$  in the first geometry  $\Omega_\varepsilon^2$ , and as  $\varepsilon^{\frac{5}{2}} \propto |\gamma_0|^{\frac{5}{4}}$  in the second geometry  $\Omega_\varepsilon^3$ . Moreover, the effectivity index is indeed almost independent from the size of the feature since it remains nearly equal to 3.10 and 3.22, respectively, for all values of  $\varepsilon$ . That is, as predicted by the theory since the estimator is both reliable (Theorem 4.6) and efficient up to oscillations (Theorem 4.8), in dimension 3, the dependence of the estimator with respect to the size of the feature is explicit. Intuitively, the two observed convergence rates of the defeaturing error and estimator are the ones expected, as it has been discussed in the 2D examples of Section 5.2.1.

### 5.3 Fillets and rounds

Classical features one finds in design for manufacturing are fillets and rounds, that allows for example the use of round-tipped end mills to cut out some material. However, fillets and rounds are non-Lipschitz feature domains. The following numerical examples analyze these types of features, and it shows that our estimator manages to capture the behavior of the defeaturing error even if the domains are not Lipschitz.

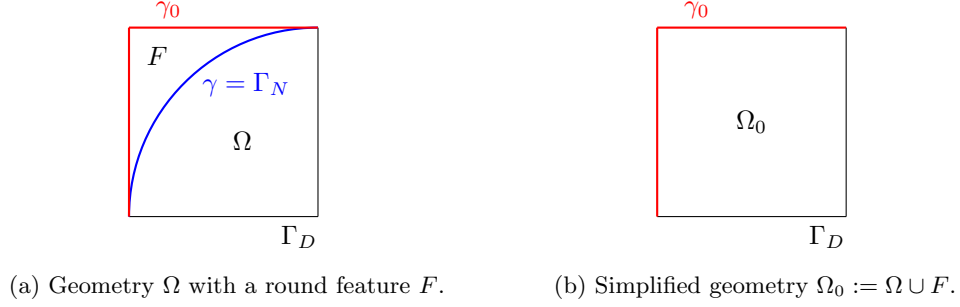


Figure 13: Geometry with a round.

$\mathcal{E}(u_0)$	$ u - u_0 _{1,\Omega}$	Effectivity index
$2.36 \cdot 10^{-1}$	$7.36 \cdot 10^{-2}$	3.21

Table 3: Results for the geometry with a round.

### 5.3.1 Round: a negative non-Lipschitz feature

Let us first consider the case of a round, that is the rounding process creates a convex domain. Let  $\Omega := \{(r \cos(\theta), r \sin(\theta)) \in \mathbb{R}^2 : 0 \leq r < 1, \frac{\pi}{2} < \theta < \pi\}$ ,  $\Omega_0 := (0, 1)^2$ , and  $F := \Omega_0 \setminus \overline{\Omega}$ , as in Figure 13. We remark that  $F$  is not a Lipschitz domain, that is this case is not covered by the presented theory. We consider Poisson problem (1) with  $f \equiv 0$  in  $\Omega$ ,  $h(x, y) := (e^x - 1)(e^{1-y} - 1)$  on

$$\Gamma_D := \{(x, 0), (1, y) \in \mathbb{R}^2 : 0 \leq x, y < 1\}.$$

and  $g \equiv 0$  on  $\Gamma_N := \partial\Omega \setminus \overline{\Gamma_D}$ . We solve the defeatured Poisson problem (3) with the same data and  $g_0 \equiv 0$  on  $\gamma_0 := \partial F \setminus \overline{\Gamma_N}$ .

The results are presented in Table 3, and we indeed have  $|u - u_0|_{1,\Omega} \lesssim \mathcal{E}(u_0)$  with a reasonably low effectivity index. This example shows that our estimator estimates well the defeaturing error even if the feature is not a Lipschitz domain, and it confirms the fact that we can indeed have a feature that is attached to the Dirichlet boundary, that is  $\bar{\gamma} \cap \Gamma_D \neq \emptyset$  but  $\gamma \cap \Gamma_D = \emptyset$ .

### 5.3.2 Fillet: a positive non-Lipschitz feature

Now, let us consider the case of a fillet, that is the filleting process creates a non-convex domain. Since the fillet  $F$  is a complex positive feature we do not want to mesh, we will consider two different feature extensions  $\tilde{F}^1$  and  $\tilde{F}^2$  containing  $F$  to solve the extension problem (6), and we will compare them. In particular, we remark again that  $F$  is not a Lipschitz domain, that is this case is not covered by the presented theory. As illustrated in Figure 14, let

$$\begin{aligned} \Omega_0 &:= \left\{ (x, y) \in \mathbb{R}^2 : 0 < x < 1, 0 < y < 1 \text{ if } 0 < x < \frac{1}{2}, 0 < y < \frac{1}{2} \text{ if } \frac{1}{2} < x < 1 \right\}, \\ \tilde{F}^1 &:= \left( \frac{1}{2}, 1 \right)^2, \\ \tilde{F}^2 &:= \tilde{F}^1 \setminus \left\{ (1 + r \cos(\theta), 1 + r \sin(\theta)) \in \mathbb{R}^2 : 0 < r < \frac{1}{4}, \pi < \theta < \frac{3\pi}{2} \right\}, \\ F &:= \tilde{F}^1 \setminus \left\{ (1 + r \cos(\theta), 1 + r \sin(\theta)) \in \mathbb{R}^2 : 0 < r < \frac{1}{2}, \pi < \theta \leq \frac{3\pi}{2} \right\}, \\ \Omega &:= \text{int}(\overline{\Omega_0} \cup \overline{F}). \end{aligned}$$

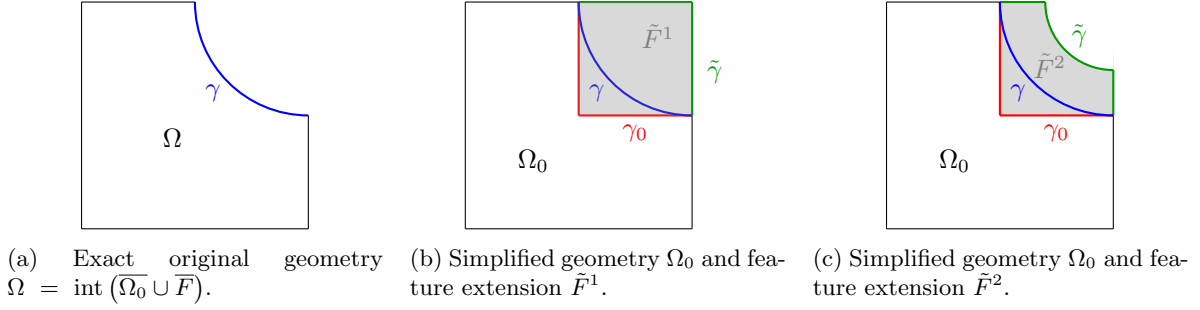


Figure 14: Geometry  $\Omega = \text{int}(\overline{\Omega_0} \cup \overline{F})$  with a fillet  $F$ , and two possible extended features.

Extension	$\mathcal{E}(u_d)$	$ u - u_d _{1,\Omega}$	$ u - u_0 _{1,\Omega_0}$	$ u - \tilde{u}_0 _{1,F}$	Effectivity index
$\tilde{F}^1$	$1.80 \cdot 10^0$	$2.92 \cdot 10^{-1}$	$1.69 \cdot 10^{-1}$	$2.39 \cdot 10^{-1}$	6.17
$\tilde{F}^2$	$1.71 \cdot 10^0$	$2.89 \cdot 10^{-1}$	$1.69 \cdot 10^{-1}$	$2.34 \cdot 10^{-1}$	5.93

Table 4: Results for the geometry with a fillet.

$\tilde{F}^1$  is the bounding box of  $F$ , it is therefore a very simple geometry but  $|\tilde{F}^1| \gg |F|$ . At the contrary,  $\tilde{F}^2$  is a little bit more complex while still being a tensor-product domain, but  $|\tilde{F}^2| \approx |F|$ .

We consider Poisson problem (1) with  $f \equiv 0$  in  $\Omega$ ,

$$h(x, y) := \cos(\pi x) + 10 \cos(5\pi x)$$

on  $\Gamma_D := \{(x, 0), (x, 1) : 0 \leq x \leq 1\}$ , and  $g \equiv 0$  on  $\Gamma_N = \partial\Omega \setminus \Gamma_D$ . We solve the defeatured Poisson problem (3) with the same data and with  $g_0 \equiv 0$  on  $\gamma_0 := \partial\Omega_0 \cap \partial F$ . Finally, we solve the Dirichlet extension problem (6) first in  $\tilde{F}^1$  and then in  $\tilde{F}^2$ , with  $\tilde{g} \equiv 0$  on  $\tilde{\gamma} := \partial\tilde{F}^1 \setminus \overline{\gamma_0}$  and  $\tilde{\gamma} := \partial\tilde{F}^2 \setminus \overline{\gamma_0}$ , respectively.

The results are presented in Table 4, and we indeed have  $|u - u_d|_{1,\Omega} \lesssim \mathcal{E}(u_d)$  with a reasonable effectivity index. Note that the effectivity index is higher in this case than in the case of a round since not only the geometry  $\Omega$  but also the feature  $F$  are simplified, respectively by  $\Omega_0$  and by  $\tilde{F}^1$  or  $\tilde{F}^2$ . Moreover, the extension  $\tilde{F}^1$  contains the extension  $\tilde{F}^2$ , and this is reflected both on the defeaturing error and on the estimator. Indeed, both the error and the estimator are larger when the considered extension is  $\tilde{F}^1$  instead of  $\tilde{F}^2$ , but the effectivity index is not affected: it is different because the shapes of  $\tilde{F}^1$  and  $\tilde{F}^2$  are different, not because an extension is bigger than the other one, as we have seen in the numerical examples of Sections 5.1 and 5.2.

## 5.4 Geometries with multiple features

Let us now consider numerical experiments that illustrate the validity of the defeaturing estimator in the case of a geometry with more than one feature.

### 5.4.1 Geometry with six features

In this example, we consider  $\Omega_0 := (0, 1)^2$ , the simplified domain of  $\Omega := \Omega_0 \setminus \bigcup_{i=1}^6 \overline{F^i}$ , where  $F^i$ ,  $i = 1, \dots, 6$  are squared features as follows (see Figure 15):

$$F^i := \{(x, y) \in \mathbb{R}^2 : -r < x - x_i < r, -r < y - y_i < r\},$$

with  $r = 0.05$  and  $(x_i, y_i)_{i=1}^6$  as in Table 5. We solve Poisson problem (1) in  $\Omega$  and its defeatured version (3) in  $\Omega_0$  with  $f := -18e^{-3(x+y)}$ ,  $h := e^{-3(x+y)}$  on

$$\Gamma_D = \{(x, 0), (0, y) \in \mathbb{R}^2 : 0 \leq x, y < 1\},$$

$i$	1	2	3	4	5	6
$x_i$	0.15	0.85	0.5	0.11	0.5	0.89
$y_i$	0.15	0.15	0.5	0.95	0.95	0.95

Table 5: Data for the geometry  $\Omega$  with 6-squared negative features.

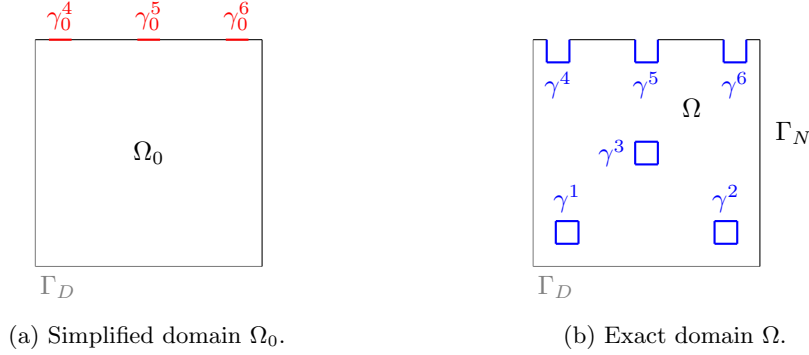


Figure 15: Simplified and exact domains with six squared features.

$g \equiv 0$  on  $\Gamma_N := \partial\Omega \setminus \overline{\Gamma_D}$ , and we choose  $g_0 \equiv 0$  on  $\gamma_0^i := \partial F^i \setminus \overline{\Gamma_N}$ , for  $i = 4, 5, 6$ .

The results are present in Table 6, and we indeed have  $|u - u_d|_{1,\Omega} \lesssim \mathcal{E}(u_d)$  with a reasonably low effectivity index. That is, as predicted by the theory in Section 4.4, the proposed estimator is able to capture the effect of defeaturing on the energy norm of the error, also when many features are present in the exact geometry and removed to create the simplified geometry. In this case, only negative (internal and boundary) features are present, but the following example show that the estimator also works in presence of multiple positive and negative features.

#### 5.4.2 Effect of the distance between features

The following numerical example is used to show that Assumption 4.11 is enough, that is one can consider features that are arbitrarily close to one another, and a positive and a negative feature can even share a part of boundary. Consider a geometry with two square features, one positive and one negative, separated by a distance  $2s \in (-0.05, 0.4)$ . That is, let  $\Omega_0 := (0, 1)^2$  and let  $\Omega_s := \text{int} \left( \overline{\Omega_0} \cup \overline{F_s^1} \setminus \overline{F_s^2} \right)$  with

$$\begin{aligned} F_s^1 &:= \{(0.4 - s, 1) + (r, r) : 0 < r < 0.1\}; \\ F_s^2 &:= \{(s, 1) + (r, -r) : 0 < r < 0.1\}, \end{aligned}$$

as illustrated in Figure 16. Features  $F_s^1$  and  $F_s^2$  satisfy Assumption 4.11 for all values of  $s$ . Then consider Poisson problem (1) with  $f \equiv 0$  in  $\Omega$ ,  $h(x, y) := 40 \cos(\pi x) + 10 \cos(5\pi x)$  on

$$\Gamma_D := \{(x, 0) \in \mathbb{R}^2 : 0 < x < 1\}$$

and  $g \equiv 0$  on  $\Gamma_N := \partial\Omega_s \setminus \overline{\Gamma_D}$ . We solve the defeatured Poisson problem (3) with the same data, and to satisfy (48) and (49), we take  $g_0 \equiv 0$  on  $\gamma_0^1 := \{(x, 1) \in \mathbb{R}^2 : 0.4 - s < x < 0.5 - s\}$  and  $\gamma_0^2 := \{(x, 1) \in \mathbb{R}^2 : 0.5 + s < x < 0.6 + s\}$ . Finally, we solve the Dirichlet extension problem (6) in  $F_s^1$ .

$\mathcal{E}(u_d)$	$ u - u_d _{1,\Omega}$	Effectivity index
$5.05 \cdot 10^{-1}$	$1.79 \cdot 10^{-1}$	2.82

Table 6: Results for the problem with six squared features.

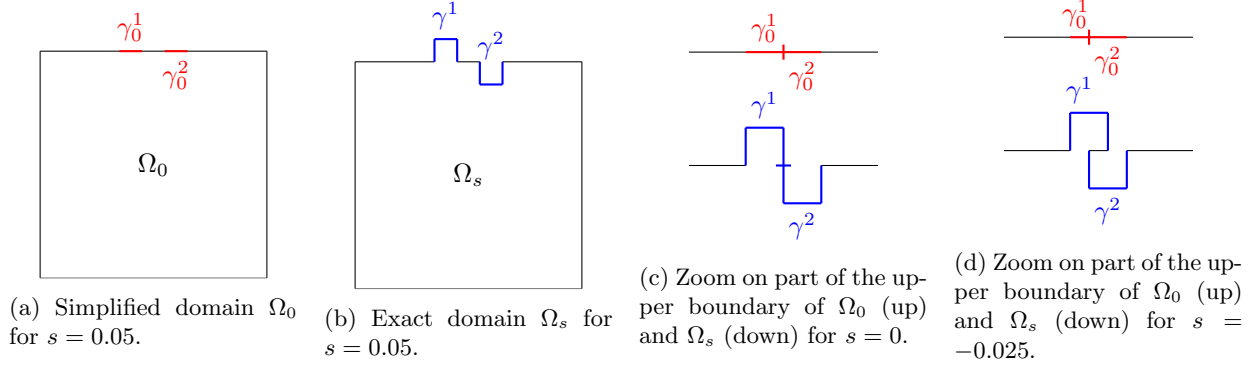


Figure 16: Simplified domains  $\Omega_0$  and exact domains  $\Omega_s$  for different values of  $s$ .

$s$	$\mathcal{E}(u_d)$	$ u - u_d _{1, \Omega_s}$	Effectivity index
$1.00 \cdot 10^{-1}$	1.55	1.49	1.04
$1.00 \cdot 10^{-4}$	1.68	1.68	1.00
$0.00 \cdot 10^0$	1.68	1.68	1.00
$-5.00 \cdot 10^{-4}$	1.78	1.68	1.05
$-4.95 \cdot 10^{-2}$	1.27	1.61	0.79

Table 7: Results for the problem with two features;  $s > 0$  corresponds to distinct features, while  $s < 0$  corresponds to features with overlapping boundaries.

We choose different values of  $s$  to consider different cases: with  $s = 10^{-1}$ , the distance between the features and the distance between  $\gamma_0^1$  and  $\gamma_0^2$  are of the same orders of magnitude as the measures of  $\gamma_0^1$  and  $\gamma_0^2$ ; with  $s = 10^{-4}$ , the distance between  $\gamma_0^1$  and  $\gamma_0^2$  is several orders of magnitude smaller than the measures of  $\gamma_0^1$  and  $\gamma_0^2$ ; with  $s = 0$ , the boundaries of the features intersect in one single point; with  $s = -5 \cdot 10^{-4}$ , the measure of the intersection between the boundaries of the features is several orders of magnitude smaller than the measures of the boundaries of the features; and with  $s = -4.95 \cdot 10^{-2}$ , the measure of the intersection between the boundaries of the features is of the same orders of magnitude as the measures of the boundaries of the features.

The results are presented in Table 7, and we indeed see that the defeaturing estimator approximates well the defeaturing error in all the different presented cases.

#### 5.4.3 Behavior with respect to the number of features

Finally, under Assumption 4.11, the effectivity of the defeaturing error estimator should not depend on the number of features present in the original geometry  $\Omega$ . To verify this, let  $\Omega_0 := (0, 1)^2$  be the fully defeatured domain, and for all  $k = 1, \dots, N = 81$ , let  $\Omega_k := \Omega_{k-1} \setminus \overline{F^k}$ , where

$$F^k := \{ \mathbf{c}^k + (r \cos(\theta), r \sin(\theta)) \in \mathbb{R}^2 : 0 \leq r < 0.03, 0 \leq \theta \leq 2\pi \},$$

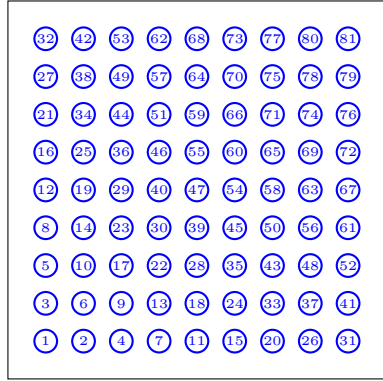
and  $\mathbf{c}^k \in \mathbb{R}^2$  are uniformly spaced between  $(0.1, 0.1)$  and  $(0.9, 0.9)$  as in Figure 17a.

Suppose that  $\Omega = \Omega_N$  is the original domain in which we solve Poisson problem (1); the solution is shown in Figure 17b. Then, we recursively solve the partially defeatured problems (3) in  $\Omega_k$  for  $k = 0, \dots, N - 1$ , and we call  $u_0^k$  its solution. We take  $f(x, y) := -18e^{-3(x+y)}$  in  $\Omega_0$ ,  $h(x, y) := e^{-3(x+y)}$  on

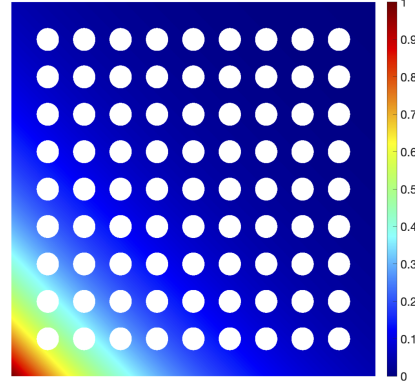
$$\Gamma_D := \{(x, 0), (0, y) \in \mathbb{R}^2 : 0 \leq x, y < 1\},$$

$$g(x, y) := -3e^{-3(x+y)} \text{ on } \partial\Omega_0 \setminus \overline{\Gamma_D} \text{ and } g \equiv 0 \text{ on } \partial F_\ell \text{ for } \ell = 1, \dots, N.$$





(a) Domain  $\Omega_N$  with  $N = 81$  features.



(b) Exact solution on  $\Omega_N$ .

Figure 17: Geometry with 81 features and corresponding exact solution.

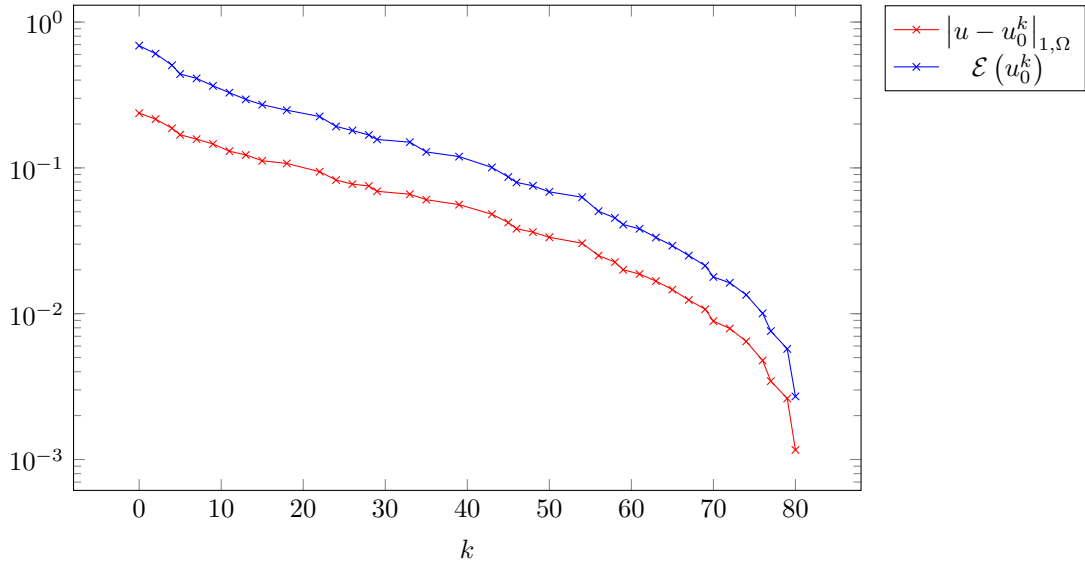


Figure 18: Behavior of the defeaturing error and estimator with respect to the number of features.

The results are presented in Figure 18. The effectivity index is almost independent from the number of features removed since it remains almost constant, between 1.99 and 2.90, for all values of  $k = 0, \dots, N - 1$ . In this example, we observe that the error monotonically increases when  $k$  decreases, because the lower is  $k$ , the higher is the number of removed features. That is, when  $k$  is low, the geometry  $\Omega$  is more simplified than when  $k$  is high, so the error is also expected to be higher. The proposed defeaturing error estimator also monotonically increases when  $k$  decreases.

## 6 Conclusions

We have introduced a novel a posteriori error estimator for analysis-aware geometric defeaturing in the context of the Laplace equation on geometries of arbitrary dimension. We have demonstrated its efficiency and reliability up to oscillations, and tested it on an extensive set of numerical experiments: in all of them, we have observed that the proposed estimator acts as an excellent approximation of the true error. We have considered geometries with either a positive or a negative feature, or with an arbitrary number of (positive and negative) features, and we have verified that our estimator is not only driven by geometrical considerations, but also by the differential problem at hand. The proposed estimator is able to weight the impact of defeaturing in energy norm, it is explicit with respect to the size of the geometrical features, and independent from the number of such features. Finally, our estimator is simple, naturally parallelizable and computationally cheap: once the solution of the defeatured problem is computed, it only requires the computation of the solution of a local extension problem on each positive feature, and boundary integrals for positive and negative features.

To conclude, we have reinforced the workflow that aims at closing the gap between design and analysis, the primary objective of isogeometric analysis, by mathematically formalizing geometric defeaturing in a way that takes into account the underlying analysis. In this paper, the analysis is performed in continuous spaces. A natural extension of our work is to develop a fully numerical scheme for analysis-aware defeaturing. This will be the subject of our subsequent work.

## A Appendix

In this section, we state lemmas that are used throughout the paper.

**Lemma A.1** (Poincaré I) *Let  $\omega$  be an  $(n - 1)$ -dimensional manifold in  $\mathbb{R}^n$  that is isotropic according to Definition 3.1. Then for all  $v \in H^{\frac{1}{2}}(\omega)$ ,*

$$\|v - \bar{v}\|_{0,\omega} \lesssim |\omega|^{\frac{1}{2(n-1)}} |v|_{\frac{1}{2},\omega},$$

where  $\bar{v} := \frac{1}{|\omega|} \int_{\omega} v \, ds$  is the average of  $v$  on  $\omega$ .

*Proof.* Let  $v \in H^{\frac{1}{2}}(\omega)$ . Recall that since  $\omega$  is an  $(n - 1)$ -dimensional manifold in  $\mathbb{R}^n$ , then

$$|v|_{\frac{1}{2},\omega}^2 = \int_{\omega} \int_{\omega} \frac{(v(x) - v(y))^2}{|x - y|^n} \, dx \, dy.$$

Moreover, let  $\tilde{\Omega}$  be the set of connected components of  $\omega$ , and let  $\tilde{\omega}_{\max} := \arg \max_{\tilde{\omega} \in \tilde{\Omega}} (\text{diam}(\tilde{\omega}))$ . Then since  $\omega$  is isotropic,

$$\text{diam}(\text{hull}(\omega)) \lesssim \text{diam}(\tilde{\omega}_{\max}) \lesssim |\tilde{\omega}_{\max}|^{\frac{1}{n-1}} \leq |\omega|^{\frac{1}{n-1}}.$$

Therefore,

$$\begin{aligned}
\|v - \bar{v}\|_{0,\omega}^2 &= \int_{\omega} \left( v(x) - \frac{1}{|\omega|} \int_{\omega} v(y) dy \right)^2 dx = \frac{1}{|\omega|^2} \int_{\omega} \left[ \int_{\omega} (v(x) - v(y)) dy \right]^2 dx \\
&\leq \frac{1}{|\omega|^2} \int_{\omega} \left[ |\omega| \int_{\omega} (v(x) - v(y))^2 dy \right] dx \\
&= \frac{1}{|\omega|} \int_{\omega} \int_{\omega} \frac{(v(x) - v(y))^2}{|x - y|^n} |x - y|^n dy dx \\
&\leq \frac{\text{diam}(\text{hull}(\omega))^n}{|\omega|} \int_{\omega} \int_{\omega} \frac{(v(x) - v(y))^2}{|x - y|^n} dy dx = |\omega|^{\frac{1}{n-1}} \|v\|_{\frac{1}{2},\omega}^2.
\end{aligned}$$

□

**Lemma A.2** (Poincaré II) *Let  $\omega$  be an  $(n-1)$ -dimensional manifold in  $\mathbb{R}^n$  that is isotropic according to Definition 3.1. Let  $\tilde{\Omega}$  be the set of connected components of  $\omega$ , then for all  $v \in H_{00}^{\frac{1}{2}}(\omega)$ ,*

$$\|v\|_{0,\omega} \lesssim \max_{\tilde{\omega} \in \tilde{\Omega}} (|\tilde{\omega}|)^{\frac{1}{2(n-1)}} \|v\|_{H_{00}^{\frac{1}{2}}(\omega)}.$$

*Proof.* Let  $D \subset \mathbb{R}^n$  and  $\varphi \subset \mathbb{R}^n$  such that  $\partial D = \bar{\omega} \cup \bar{\varphi}$  and  $\omega \cap \varphi = \emptyset$ . Let  $v \in H_{00}^{\frac{1}{2}}(\omega)$ . Then for all  $\tilde{\omega} \in \tilde{\Omega}$ ,  $v|_{\tilde{\omega}} \in H_{00}^{\frac{1}{2}}(\tilde{\omega})$  and  $\sum_{\tilde{\omega} \in \tilde{\Omega}} \|v|_{\tilde{\omega}}\|_{H_{00}^{\frac{1}{2}}(\tilde{\omega})}^2 \leq \|v\|_{H_{00}^{\frac{1}{2}}(\omega)}^2$ . Indeed, for all  $\tilde{\omega} \in \tilde{\Omega}$ , let  $v^* \in H^{\frac{1}{2}}(\partial D)$  and  $v|_{\tilde{\omega}}^* \in H^{\frac{1}{2}}(\partial D)$  be the extension of  $v$  and  $v|_{\tilde{\omega}}$  by 0. Then for all  $x, y \in \partial D$ ,

$$\begin{aligned}
\sum_{\tilde{\omega} \in \tilde{\Omega}} (v|_{\tilde{\omega}}^*(x) - v|_{\tilde{\omega}}^*(y))^2 &\leq \sum_{\tilde{\omega}_1 \in \tilde{\Omega}} \sum_{\tilde{\omega}_2 \in \tilde{\Omega}} (v|_{\tilde{\omega}_1}^*(x) - v|_{\tilde{\omega}_2}^*(y))^2 \\
&\lesssim \left( \sum_{\tilde{\omega}_1 \in \tilde{\Omega}} v|_{\tilde{\omega}_1}^*(x) - \sum_{\tilde{\omega}_2 \in \tilde{\Omega}} v|_{\tilde{\omega}_2}^*(y) \right)^2 = (v^*(x) - v^*(y))^2.
\end{aligned}$$

Consequently,

$$\begin{aligned}
\sum_{\tilde{\omega} \in \tilde{\Omega}} \left( |v|_{\tilde{\omega}}|_{\frac{1}{2},\tilde{\omega}}^2 + |v|_{\tilde{\omega}}|_{H_{00}^{\frac{1}{2}}(\tilde{\omega})}^2 \right) &= \sum_{\tilde{\omega} \in \tilde{\Omega}} |v|_{\tilde{\omega}}|_{\frac{1}{2},\partial D}^2 = \sum_{\tilde{\omega} \in \tilde{\Omega}} \int_{\partial D} \int_{\partial D} \frac{(v|_{\tilde{\omega}}^*(x) - v|_{\tilde{\omega}}^*(y))^2}{|x - y|^n} dx dy \\
&\lesssim \int_{\partial D} \int_{\partial D} \frac{(v^*(x) - v^*(y))^2}{|x - y|^n} dx dy \\
&= |v^*|_{\frac{1}{2},\partial D}^2 = |v|_{\frac{1}{2},\omega}^2 + |v|_{H_{00}^{\frac{1}{2}}(\omega)}^2.
\end{aligned} \tag{58}$$

Moreover, from [45, Proposition 2.4], since  $\omega$  is isotropic, for all  $\tilde{\omega} \in \tilde{\Omega}$ ,

$$\|v|_{\tilde{\omega}}\|_{0,\tilde{\omega}}^2 \lesssim |\tilde{\omega}|^{\frac{1}{n-1}} |v|_{\tilde{\omega}}|_{\frac{1}{2},\partial D}^2 = |\tilde{\omega}|^{\frac{1}{n-1}} \left( |v|_{\tilde{\omega}}|_{\frac{1}{2},\omega}^2 + |v|_{\tilde{\omega}}|_{H_{00}^{\frac{1}{2}}(\tilde{\omega})}^2 \right). \tag{59}$$

Therefore, from (58) and (59),

$$\|w\|_{0,\omega}^2 = \sum_{\tilde{\omega} \in \tilde{\Omega}} \|v|_{\tilde{\omega}}\|_{0,\tilde{\omega}}^2 \lesssim \sum_{\tilde{\omega} \in \tilde{\Omega}} |\tilde{\omega}|^{\frac{1}{n-1}} \left( |v|_{\tilde{\omega}}|_{\frac{1}{2},\omega}^2 + |v|_{\tilde{\omega}}|_{H_{00}^{\frac{1}{2}}(\tilde{\omega})}^2 \right) \lesssim \max_{\tilde{\omega} \in \tilde{\Omega}} (|\tilde{\omega}|)^{\frac{1}{n-1}} \|v\|_{H_{00}^{\frac{1}{2}}(\omega)}^2.$$

□

**Lemma A.3** (Inverse inequality) *Let  $\omega$  be an open  $(n-1)$ -dimensional manifold in  $\mathbb{R}^n$  that is isotropic and regular according to Definitions 3.1 and 3.2, and let  $\mathbf{m} \in \mathbb{N}^n$ . Then for all  $p \in \mathbb{Q}_{\mathbf{m},0}^{\text{pw}}(\omega)$ ,*

$$|\omega|^{\frac{1}{2(n-1)}} \|p\|_{0,\omega} \lesssim \|p\|_{H_{00}^{-1/2}(\omega)},$$

where the hidden constant increases with  $\mathbf{m}$ .

*Proof.* For all  $q \in \mathbb{Q}_{\mathbf{m},0}^{\text{pw}}(\omega) \subset H_0^1(\omega)$ , the following inverse estimate is well known (see [46, Theorem 3.2], for example): with the notation of Definition 3.2, for all  $\ell = 1, \dots, L_\omega$ ,

$$\|q|_{\omega_\ell}\|_{1,\omega_\ell} \lesssim |\omega_\ell|^{-\frac{1}{n-1}} \|q|_{\omega_\ell}\|_{0,\omega_\ell},$$

and the hidden constant increases with  $\mathbf{m}$ . Therefore, since  $\omega$  is isotropic and shape regular,

$$|q|_{1,\omega} \lesssim \|q\|_{1,\omega} \lesssim \max_{\ell=1,\dots,L_\omega} \left( |\omega_\ell|^{-\frac{1}{n-1}} \right) \|q\|_{0,\omega} \lesssim |\omega|^{-\frac{1}{n-1}} \|q\|_{0,\omega}.$$

Moreover, from [47], we know that the interpolation space  $[H_0^1(\omega), L^2(\omega)]_{\frac{1}{2}} = H_{00}^{\frac{1}{2}}(\omega)$  (see also [48, Theorem 11.7]). Therefore, from [48, Proposition 2.3], for all  $q \in \mathbb{Q}_{\mathbf{m},0}^{\text{pw}}(\omega)$ ,

$$\|q\|_{H_{00}^{1/2}(\omega)} \lesssim |q|_{1,\omega}^{\frac{1}{2}} \|q\|_{0,\omega}^{\frac{1}{2}} \lesssim |\omega|^{-\frac{1}{2(n-1)}} \|q\|_{0,\omega}.$$

Consequently, for all  $p \in \mathbb{Q}_{\mathbf{m},0}^{\text{pw}}(\omega) \subset H_{00}^{-\frac{1}{2}}(\omega)$ , since  $\mathbb{Q}_{\mathbf{m},0}^{\text{pw}}(\omega) \subset H_{00}^{\frac{1}{2}}(\omega)$ ,

$$\begin{aligned} \|p\|_{0,\omega} &= \frac{\int_{\omega} p^2 \, ds}{\|p\|_{0,\omega}} \leq \sup_{\substack{q \in \mathbb{Q}_{\mathbf{m},0}^{\text{pw}}(\omega) \\ q \neq 0}} \frac{\int_{\omega} pq \, ds}{\|q\|_{0,\omega}} \lesssim |\omega|^{-\frac{1}{2(n-1)}} \sup_{\substack{q \in \mathbb{Q}_{\mathbf{m},0}^{\text{pw}}(\omega) \\ q \neq 0}} \frac{\int_{\omega} pq \, ds}{\|q\|_{H_{00}^{1/2}(\omega)}} \\ &\leq |\omega|^{-\frac{1}{2(n-1)}} \sup_{\substack{v \in H_{00}^{1/2}(\omega) \\ v \neq 0}} \frac{\int_{\omega} pv \, ds}{\|v\|_{H_{00}^{1/2}(\omega)}} = |\omega|^{-\frac{1}{2(n-1)}} \|p\|_{H_{00}^{-1/2}(\omega)}. \end{aligned}$$

□

**Lemma A.4** *Let  $\omega$  be an  $(n-1)$ -dimensional manifold in  $\mathbb{R}^n$  that is isotropic according to Definition 3.1. Let  $\tilde{\Omega}$  be the set of connected components of  $\omega$ , then for all  $v \in L^2(\omega)$ ,*

$$\|v\|_{H_{00}^{-1/2}(\omega)} \lesssim \max_{\tilde{\omega} \in \tilde{\Omega}} (|\tilde{\omega}|)^{\frac{1}{2(n-1)}} \|v\|_{0,\omega}.$$

*Proof.* Since  $H_{00}^{-\frac{1}{2}}(\omega)$  is the dual space of  $H_{00}^{\frac{1}{2}}(\omega)$ , then by Lemma A.2, we obtain

$$\begin{aligned} \|v\|_{H_{00}^{-1/2}(\omega)} &= \sup_{\substack{z \in H_{00}^{1/2}(\omega) \\ z \neq 0}} \frac{\int_{\omega} vz \, ds}{\|z\|_{H_{00}^{1/2}(\omega)}} \leq \sup_{\substack{z \in H_{00}^{1/2}(\omega) \\ z \neq 0}} \frac{\|v\|_{0,\omega} \|z\|_{0,\omega}}{\|z\|_{H_{00}^{1/2}(\omega)}} \\ &\lesssim \sup_{\substack{z \in H_{00}^{1/2}(\omega) \\ z \neq 0}} \frac{\|v\|_{0,\omega} \max_{\tilde{\omega} \in \tilde{\Omega}} (|\tilde{\omega}|)^{\frac{1}{2(n-1)}} \|z\|_{H_{00}^{1/2}(\omega)}}{\|z\|_{H_{00}^{1/2}(\omega)}} \\ &= \max_{\tilde{\omega} \in \tilde{\Omega}} (|\tilde{\omega}|)^{\frac{1}{2(n-1)}} \|v\|_{0,\omega}. \end{aligned}$$

□

## Acknowledgment

The authors gratefully acknowledge the support of the European Research Council, via the ERC AdG project CHANGE n.694515. R. Vázquez Hernández also thanks the support of the Swiss National Science Foundation via the project HOGAEMS n.200021\_188589.

## References

- [1] T. Hughes, J. Cottrell, and Y. Bazilevs, “Isogeometric analysis: CAD, finite elements, NURBS, exact geometry, and mesh refinement,” *Computer Methods in Applied Mechanics and Engineering*, vol. 194, pp. 4135–4195, 2005.
- [2] J. Cottrell, T. Hughes, and Y. Bazilevs, *Isogeometric analysis: towards integration of CAD and FEA*. Wiley, 2009.
- [3] T. Hughes, “Isogeometric analysis: Progress and challenges,” *Computer Methods in Applied Mechanics and Engineering*, vol. 316, p. 1, 2017. Special Issue on Isogeometric Analysis: Progress and Challenges.
- [4] L. B. da Veiga, A. Buffa, G. Sangalli, and R. Vázquez, “Mathematical analysis of variational isogeometric methods,” *Acta Numerica*, vol. 23, p. 157287, 2014.
- [5] Y. Bazilevs, L. Beirão Da Veiga, J. A. Cottrell, T. J. R. Hughes, and G. Sangalli, “Isogeometric analysis: approximation, stability and error estimates for h-refined meshes,” *Mathematical Models and Methods in Applied Sciences*, vol. 16, no. 07, pp. 1031–1090, 2006.
- [6] L. Beirão Da Veiga, A. Buffa, G. Sangalli, and R. Vázquez, “Analysis-suitable T-splines of arbitrary degree: definition, linear independence and approximation properties,” *Mathematical Models and Methods in Applied Sciences*, vol. 23, no. 11, pp. 1979–2003, 2013.
- [7] A. Buffa and C. Giannelli, “Adaptive isogeometric methods with hierarchical splines: error estimator and convergence,” *Mathematical Models and Methods in Applied Sciences*, vol. 26, no. 01, pp. 1–25, 2016.
- [8] A. Buffa and C. Giannelli, “Adaptive isogeometric methods with hierarchical splines: optimality and convergence rates,” *Mathematical Models and Methods in Applied Sciences*, vol. 27, no. 14, pp. 2781–2802, 2017.
- [9] A. Buffa and E. M. Garau, “A posteriori error estimators for hierarchical B-spline discretizations,” *Mathematical Models and Methods in Applied Sciences*, vol. 28, no. 08, pp. 1453–1480, 2018.
- [10] A. Buffa, R. H. Vázquez, G. Sangalli, and L. Beiro da Veiga, “Approximation estimates for isogeometric spaces in multipatch geometries,” *Numerical Methods for Partial Differential Equations*, vol. 31, no. 2, pp. 422–438, 2015.
- [11] B. Marussig and T. J. R. Hughes, “A review of trimming in isogeometric analysis: Challenges, data exchange and simulation aspects,” *Archives of Computational Methods in Engineering*, vol. 25, pp. 1059–1127, Nov 2018.
- [12] R. Schmidt, R. Wehner, and K.-U. Bletzinger, “Isogeometric analysis of trimmed nurbs geometries,” *Computer Methods in Applied Mechanics and Engineering*, vol. 241-244, pp. 93 – 111, 2012.
- [13] P. Antolin, A. Buffa, and M. Martinelli, “Isogeometric analysis on V-reps: first results,” *Computer Methods in Applied Mechanics and Engineering*, vol. 355, pp. 976–1002, 2019.
- [14] P. Antolin, A. Buffa, R. Puppi, and X. Wei, “Overlapping multi-patch isogeometric method with minimal stabilization,” *arXiv:1912.06400*, 2019.
- [15] S. Kargaran, B. Jüttler, S. Kleiss, A. Mantzavlaris, and T. Takacs, “Overlapping multi-patch structures in isogeometric analysis,” *Computer Methods in Applied Mechanics and Engineering*, vol. 356, pp. 325 – 353, 2019.
- [16] B.-Q. Zuo, Z.-D. Huang, Y.-W. Wang, and Z.-J. Wu, “Isogeometric analysis for CSG models,” *Computer Methods in Applied Mechanics and Engineering*, vol. 285, pp. 102 – 124, 2015.

- [17] M. Breitenberger, A. Apostolatos, B. Philipp, R. Wüchner, and K.-U. Bletzinger, “Analysis in computer aided design: Nonlinear isogeometric B-Rep analysis of shell structures,” *Computer Methods in Applied Mechanics and Engineering*, vol. 284, pp. 401–457, 2015.
- [18] T. Teschemacher, A. Bauer, T. Oberbichler, M. Breitenberger, R. Rossi, R. Wüchner, and K.-U. Bletzinger, “Realization of CAD-integrated shell simulation based on isogeometric B-Rep analysis,” *Advanced Modeling and Simulation in Engineering Sciences*, vol. 5, no. 1, p. 19, 2018.
- [19] M. Elhaddad, N. Zander, S. Kollmannsberger, A. Shadavakhsh, V. Nbel, and E. Rank, “Finite cell method: High-order structural dynamics for complex geometries,” *International Journal of Structural Stability and Dynamics*, vol. 15, no. 07, p. 1540018, 2015.
- [20] E. Rank, M. Ruess, S. Kollmannsberger, D. Schillinger, and A. Düster, “Geometric modeling, isogeometric analysis and the finite cell method,” *Computer Methods in Applied Mechanics and Engineering*, vol. 249, pp. 104–115, 2012.
- [21] D. Schillinger, L. Dede, M. A. Scott, J. A. Evans, M. J. Borden, E. Rank, and T. J. Hughes, “An isogeometric design-through-analysis methodology based on adaptive hierarchical refinement of nurbs, immersed boundary methods, and t-spline cad surfaces,” *Computer Methods in Applied Mechanics and Engineering*, vol. 249, pp. 116–150, 2012.
- [22] A. Thakur, A. G. Banerjee, and S. K. Gupta, “A survey of CAD model simplification techniques for physics-based simulation applications,” *Computer-Aided Design*, vol. 41, no. 2, pp. 65–80, 2009.
- [23] L. Fine, L. Remondini, and J.-C. Leon, “Automated generation of FEA models through idealization operators,” *International Journal for Numerical Methods in Engineering*, vol. 49, no. 12, pp. 83–108, 2000.
- [24] N. Rahimi, P. Kerfriden, F. C. Langbein, and R. R. Martin, “CAD model simplification error estimation for electrostatics problems,” *SIAM Journal on Scientific Computing*, vol. 40, no. 1, pp. B196–B227, 2018.
- [25] R. Ferrandes, P. Marin, J.-C. Lon, and F. Giannini, “A posteriori evaluation of simplification details for finite element model preparation,” *Computers & Structures*, vol. 87, no. 1, pp. 73 – 80, 2009.
- [26] S. H. Gopalakrishnan and K. Suresh, “Feature sensitivity: a generalization of topological sensitivity,” *Finite Elements in Analysis and Design*, vol. 44, no. 11, pp. 696 – 704, 2008.
- [27] I. Turevsky, S. H. Gopalakrishnan, and K. Suresh, “Defeaturing: A posteriori error analysis via feature sensitivity,” *International journal for numerical methods in engineering*, vol. 76, no. 9, pp. 1379–1401, 2008.
- [28] K. K. Choi and N.-H. Kim, *Structural Sensitivity Analysis and Optimization 1: Linear Systems*. Springer Science & Business Media, 2005.
- [29] J. Sokolowski and A. Zochowski, “On the topological derivative in shape optimization,” *SIAM journal on control and optimization*, vol. 37, no. 4, pp. 1251–1272, 1999.
- [30] M. Li, S. Gao, and R. R. Martin, “Estimating the effects of removing negative features on engineering analysis,” *Computer-Aided Design*, vol. 43, no. 11, pp. 1402 – 1412, 2011. Solid and Physical Modeling 2011.
- [31] R. Becker and R. Rannacher, “An optimal control approach to a posteriori error estimation in finite element methods,” *Acta numerica*, vol. 10, pp. 1–102, 2001.
- [32] J. T. Oden and S. Prudhomme, “Estimation of modeling error in computational mechanics,” *Journal of Computational Physics*, vol. 182, no. 2, pp. 496–515, 2002.

- [33] J. Oden and K. S. Vemaganti, “Estimation of local modeling error and goal-oriented adaptive modeling of heterogeneous materials: I. Error estimates and adaptive algorithms,” *Journal of Computational Physics*, vol. 164, no. 1, pp. 22 – 47, 2000.
- [34] K. Vemaganti, “Modelling error estimation and adaptive modelling of perforated materials,” *International Journal for Numerical Methods in Engineering*, vol. 59, no. 12, pp. 1587–1604, 2004.
- [35] S. Repin, S. Sauter, and A. Smolianski, “A posteriori error estimation for the dirichlet problem with account of the error in the approximation of boundary conditions,” *Computing*, vol. 70, no. 3, pp. 205–233, 2003.
- [36] M. Li and S. Gao, “Estimating defeaturing-induced engineering analysis errors for arbitrary 3D features,” *Computer-Aided Design*, vol. 43, no. 12, pp. 1587 – 1597, 2011.
- [37] M. Li, S. Gao, and K. Zhang, “A goal-oriented error estimator for the analysis of simplified designs,” *Computer Methods in Applied Mechanics and Engineering*, vol. 255, pp. 89 – 103, 2013.
- [38] M. Li, S. Gao, and R. R. Martin, “Engineering analysis error estimation when removing finite-sized features in nonlinear elliptic problems,” *Computer-Aided Design*, vol. 45, no. 2, pp. 361 – 372, 2013. Solid and Physical Modeling 2012.
- [39] K. Zhang, M. Li, and J. Li, “Estimation of impacts of removing arbitrarily constrained domain details to the analysis of incompressible fluid flows,” *Communications in Computational Physics*, vol. 20, no. 4, p. 944968, 2016.
- [40] C. Carstensen and S. Sauter, “A posteriori error analysis for elliptic PDEs on domains with complicated structures,” *Numer. Math.*, vol. 96, no. 4, pp. 691–721, 2004.
- [41] P. Grisvard, *Elliptic Problems in Nonsmooth Domains*. Society for Industrial and Applied Mathematics, 2011.
- [42] P. Clément, “Approximation by finite element functions using local regularization,” *ESAIM: Mathematical Modelling and Numerical Analysis - Modélisation Mathématique et Analyse Numérique*, vol. 9, no. R2, pp. 77–84, 1975.
- [43] C. Bernardi and V. Girault, “A local regularization operator for triangular and quadrilateral finite elements,” *SIAM J. Numer. Anal.*, vol. 35, p. 18931916, Oct. 1998.
- [44] R. Vázquez, “A new design for the implementation of isogeometric analysis in Octave and Matlab: GeoPDEs 3.0,” *Computers & Mathematics with Applications*, vol. 72, no. 3, pp. 523–554, 2016.
- [45] G. Acosta and J. P. Borthagaray, “A fractional Laplace equation: regularity of solutions and finite element approximations,” *SIAM Journal on Numerical Analysis*, vol. 55, no. 2, pp. 472–495, 2017.
- [46] I. G. Graham, W. Hackbusch, and S. A. Sauter, “Finite elements on degenerate meshes: inverse-type inequalities and applications,” *IMA Journal of Numerical Analysis*, vol. 25, pp. 379–407, Apr. 2005.
- [47] H. Triebel, “Spaces of Besov-Hardy-Sobolev type on complete Riemannian manifolds,” *Ark. Mat.*, vol. 24, pp. 299–337, 12 1985.
- [48] J. L. Lions and E. Magenes, *Non-Homogeneous Boundary Value Problems and Applications*, vol. 1. Springer-Verlag, 1973.